de Vaucouleurs' $R^{1/4}$ law for ellipticals and bulges

A good fit to the light profile of many ellipticals and bulges:

$$\ln I(R) = \ln I_e + 7.669 \left[1 - \left(\frac{R}{R_e}\right)^{1/4}\right]$$

I = surface brightness

R = projected radius

R_e = effective radius enclosing 1/2 of light

$$\int_0^{R_e} I(R) r dr = \frac{1}{2} \int_0^{\infty} I(R) r dr.$$

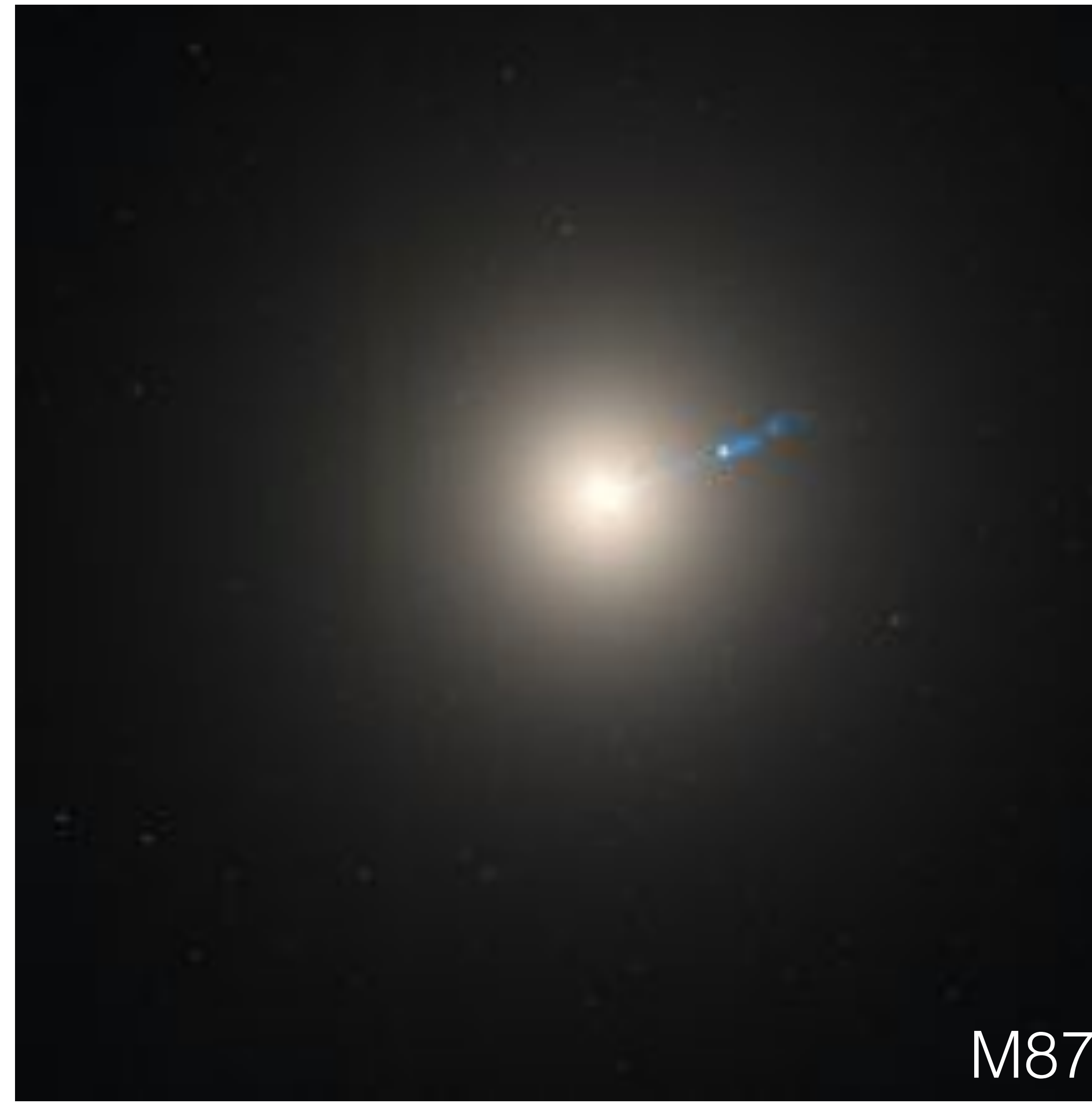

Sérsic profile

Generalization of de Vaucouleurs' $R^{1/4}$ law

$$\ln\ I(R) = \ln\ I_0 - kR^{1/n}$$

n=Sérsic index (=4 for $R^{1/4}$)

More luminous galaxies tend to have larger n

n=1 gives exponential profile

$$I(R) \propto e^{-kR}$$

which is a good approximation to many spirals

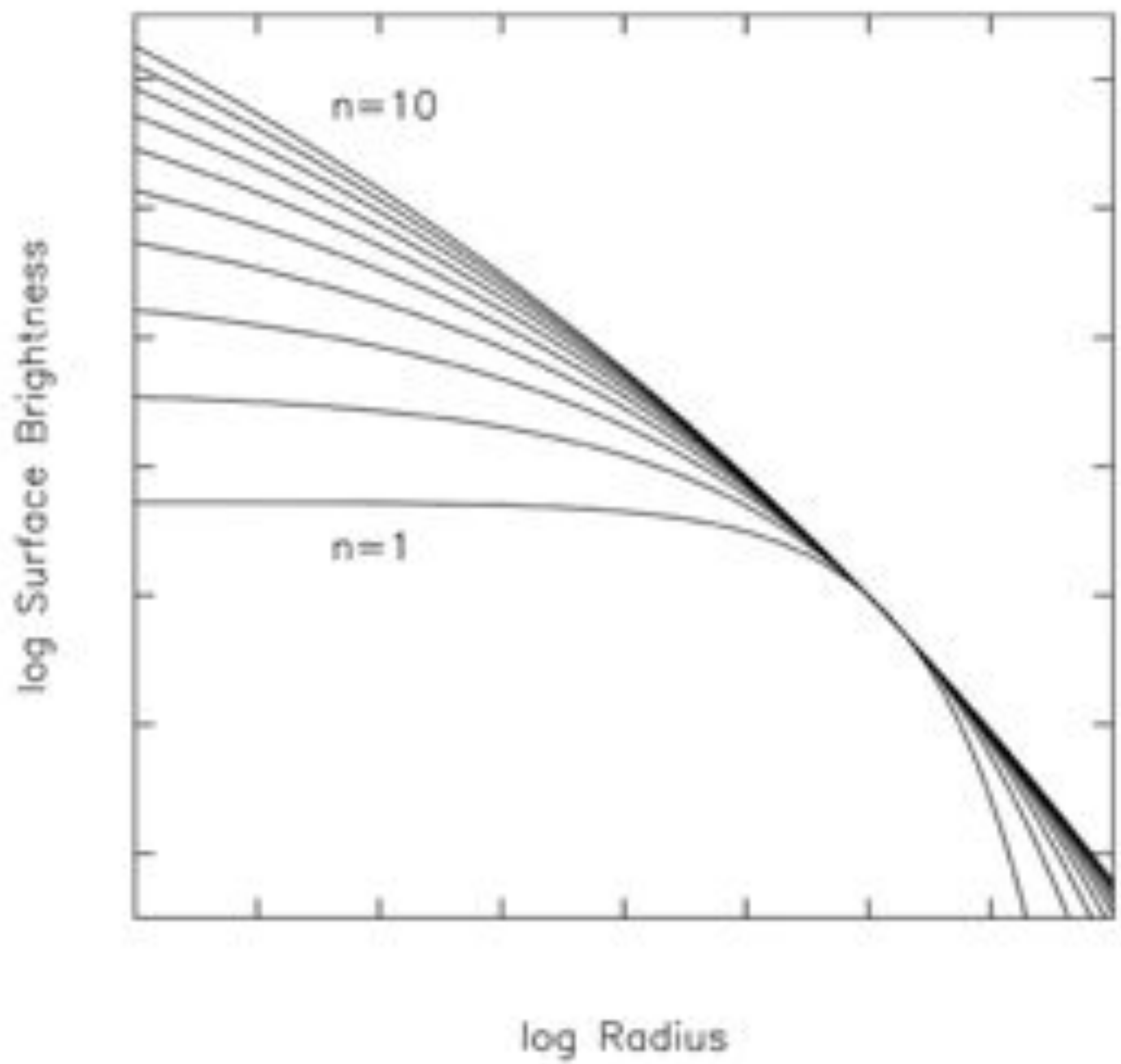

Hernquist profile

Sky projection is close to $R^{1/4}$ law, but 3D mass distribution is analytically tractable (unlike $R^{1/4}$):

$$\rho(r) = \frac{M}{2\pi}\frac{a}{r}\frac{1}{(r+a)^3}$$

M = total mass
a = scale radius

Very convenient for theoretical models of ellipticals and bulges

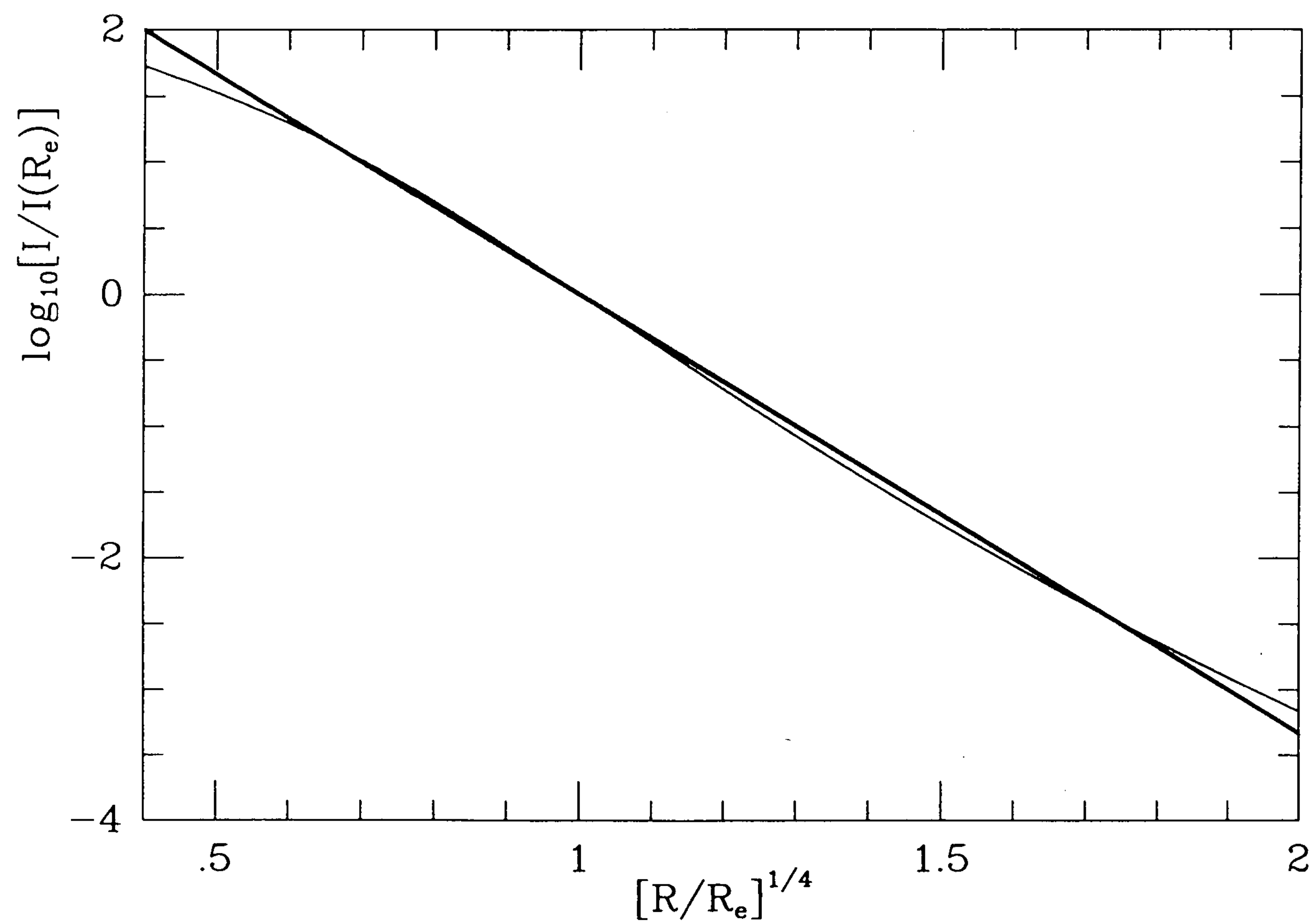

FIG. 4.—Surface brightness profiles for the $R^{1/4}$ law (*thick curve*) and the present model (*thin curve*) as a function of $(R/R_e)^{1/4}$. Surface brightness is normalized to its value at R_e where R_e refers separately to the effective radii of the two models.

Hernquist 90

Cosmological *N*-body simulations
and
dark matter halos

The standard Λ Cold Dark Matter cosmology

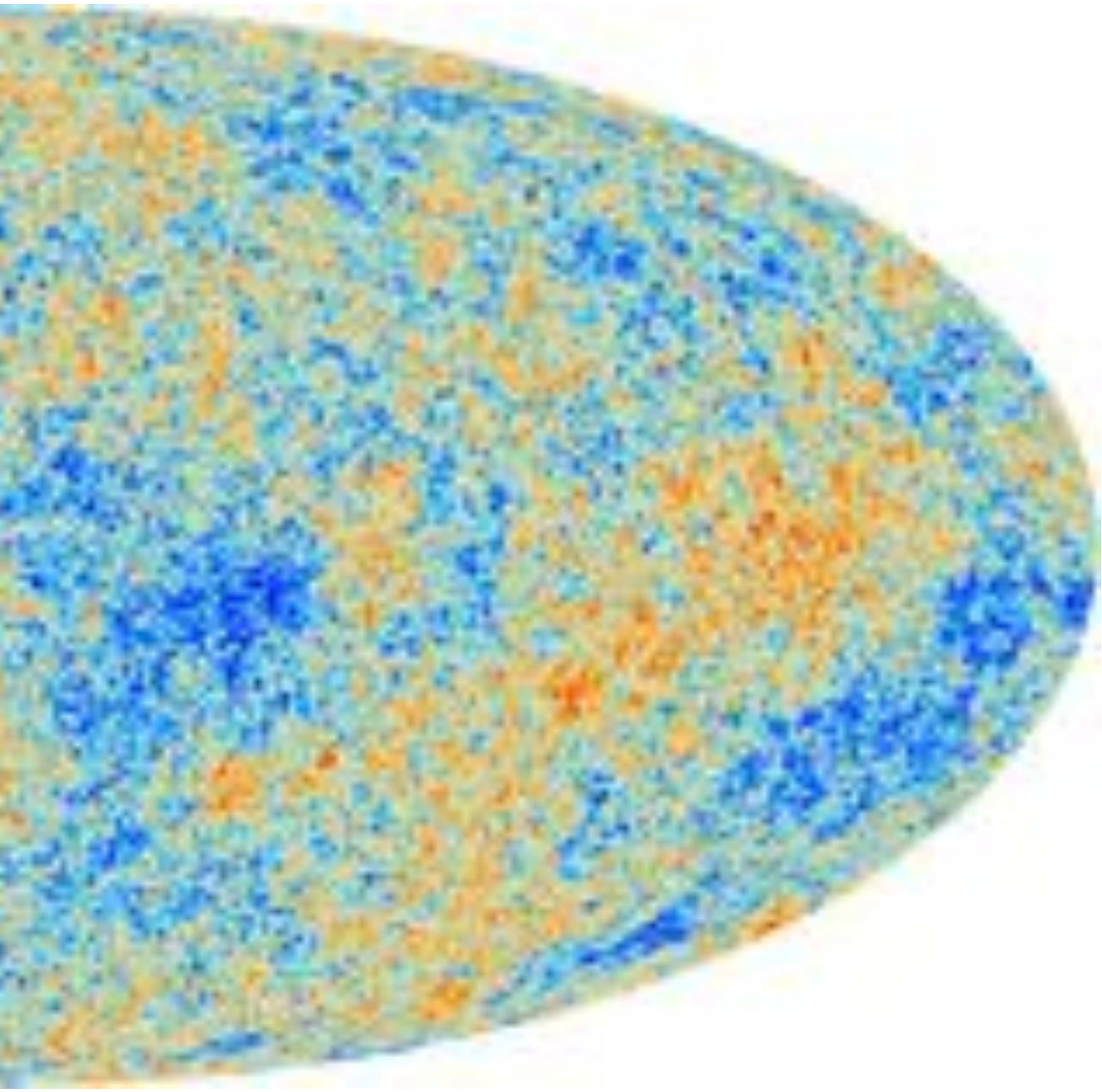

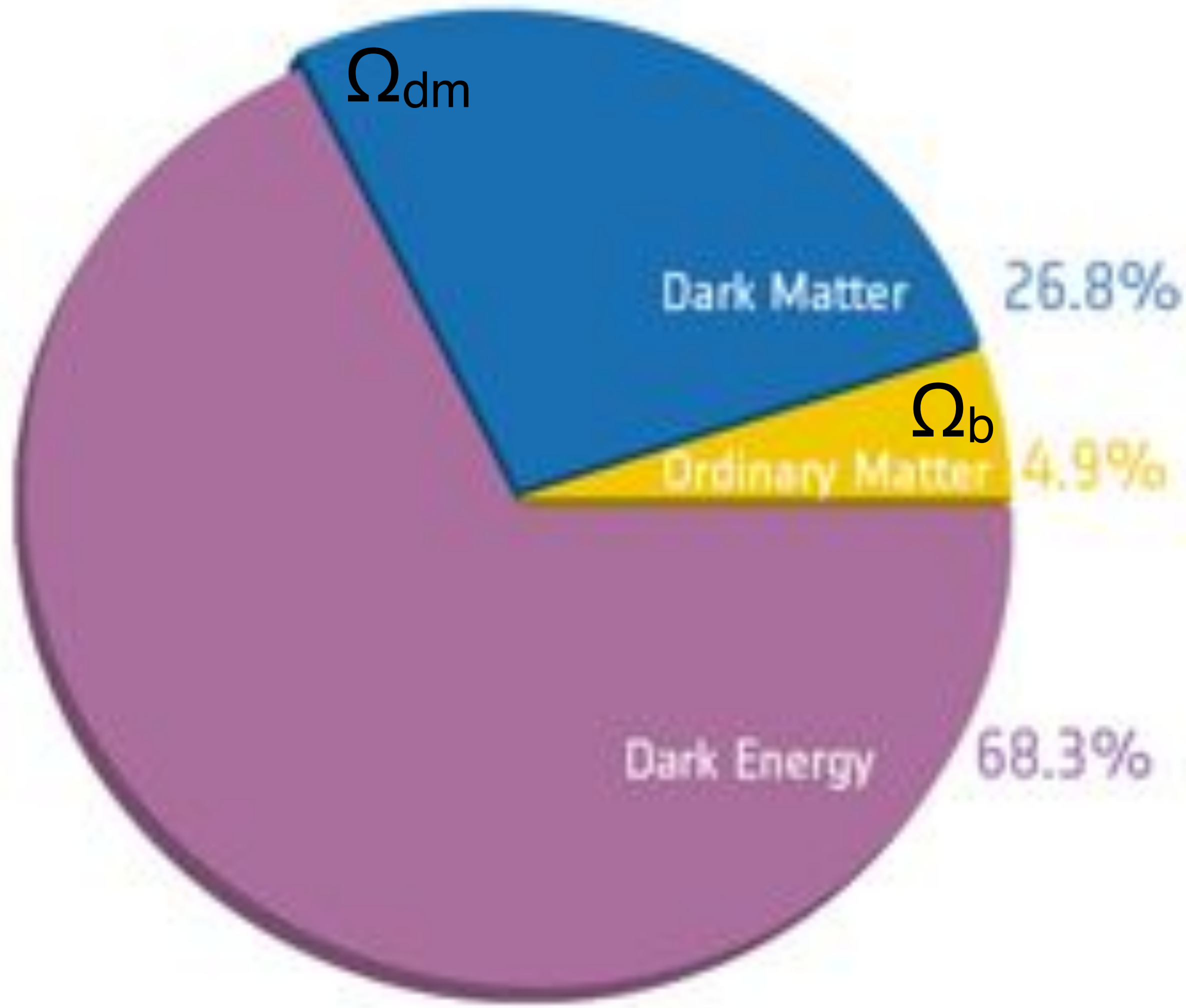

Combined with other astronomical measurements, the cosmic microwave background tells us:

- spectrum of initial density fluctuations
- what the Universe is made out of
- how old it is and how it has expanded in time

Initial conditions for cosmological simulations

Microwave sky

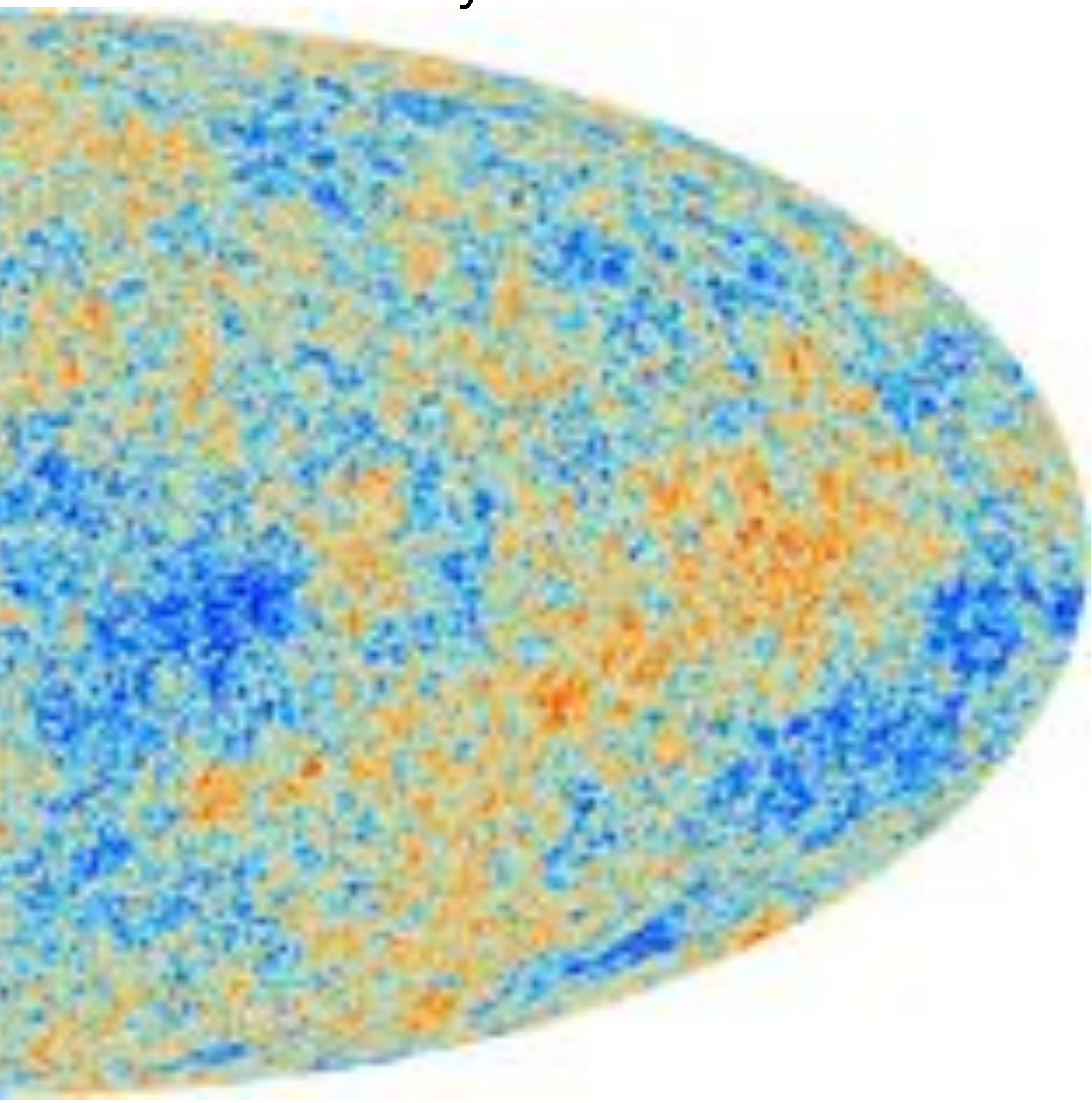

Simulation ICs

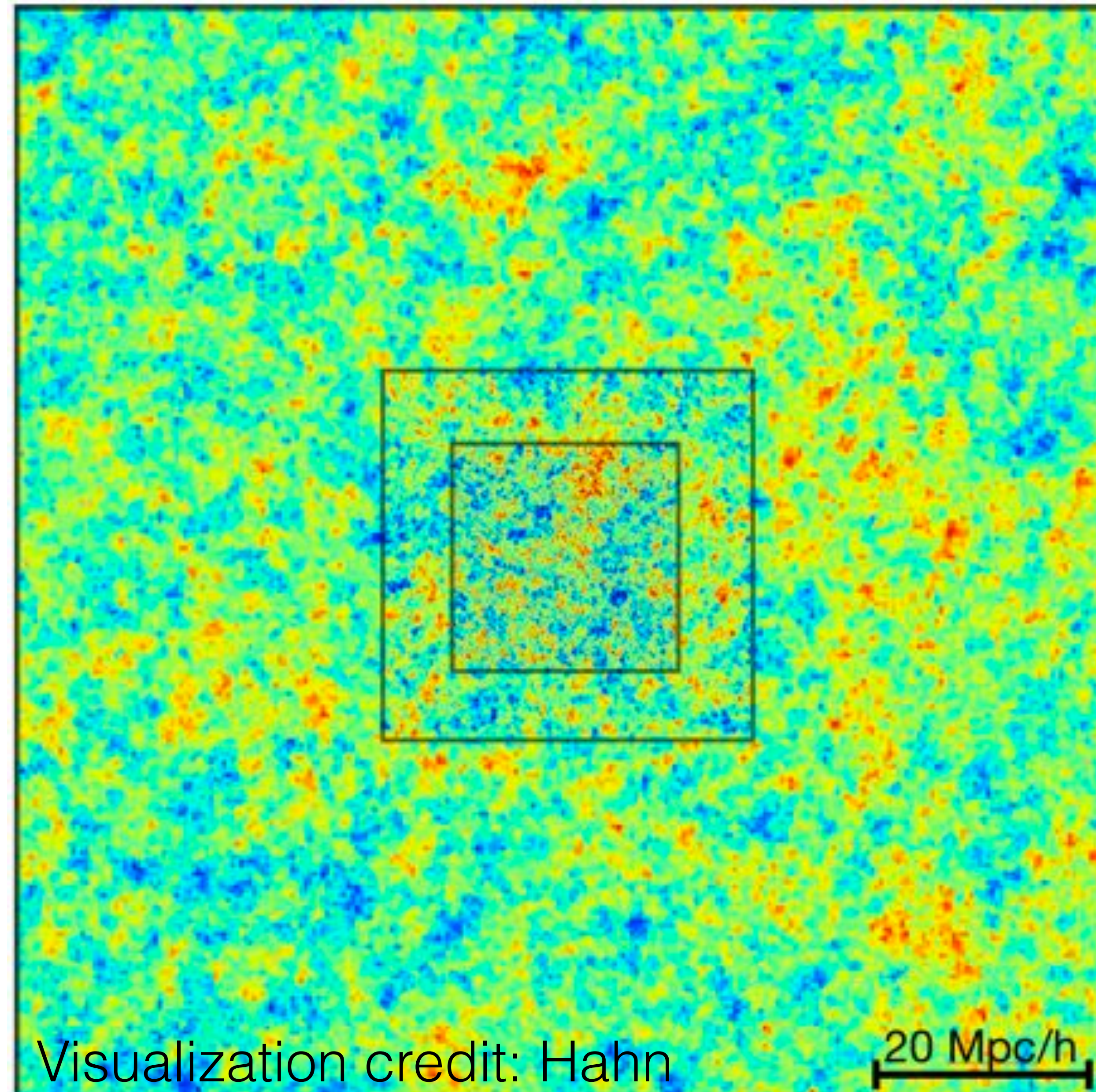

Gaussian random field filtered with transfer function to model early Universe physics (photon-baryon interactions)

N-body simulations

- Discretize mass with *N* particles
    - in cosmology, usually tree or particle-mesh methods to solve Poisson's equation

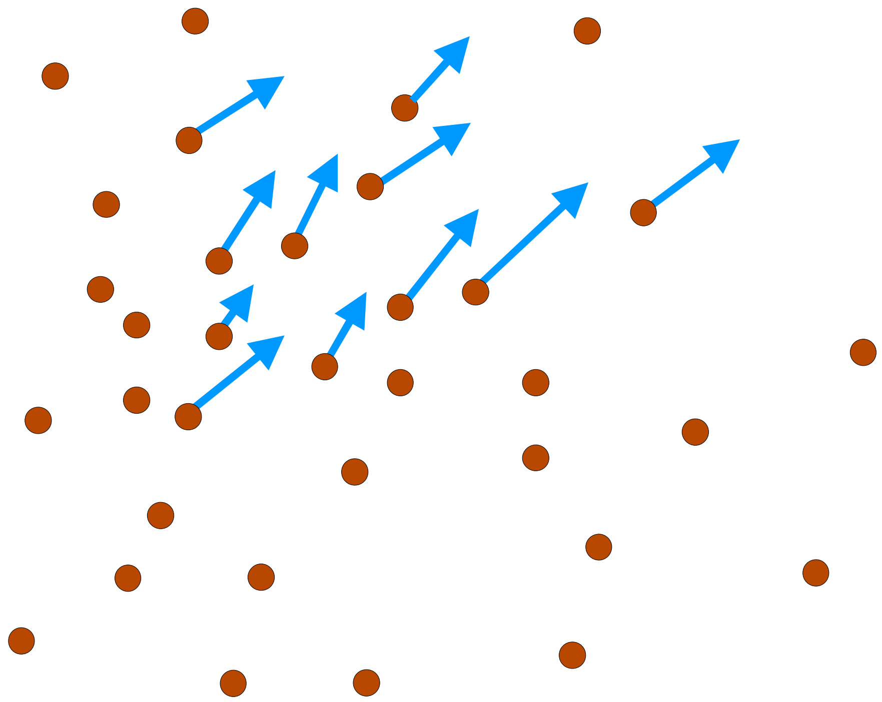

- Naturally adaptive in cosmology

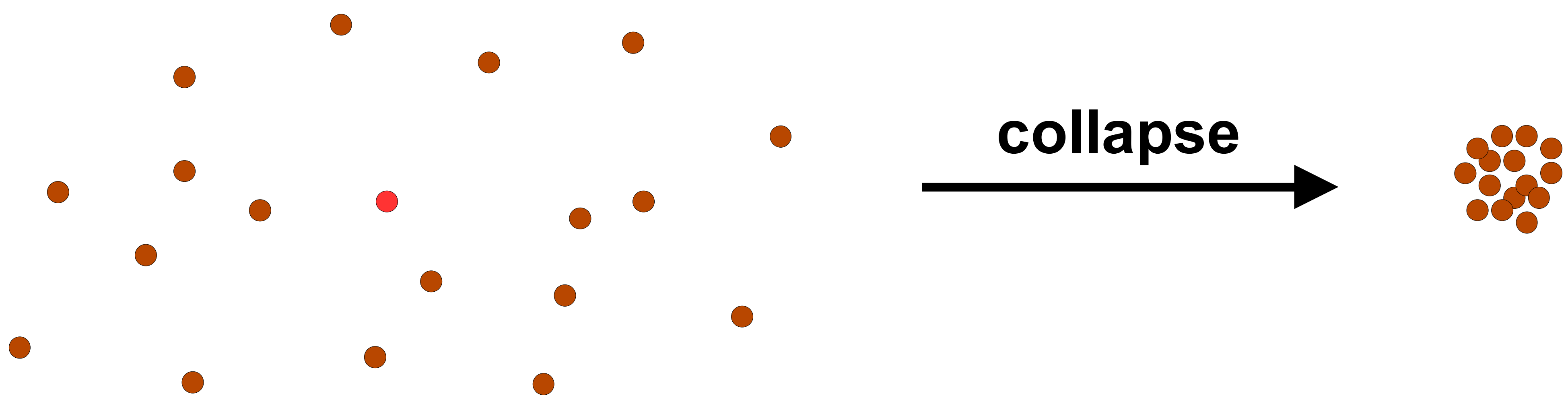

History of *N*-body simulations

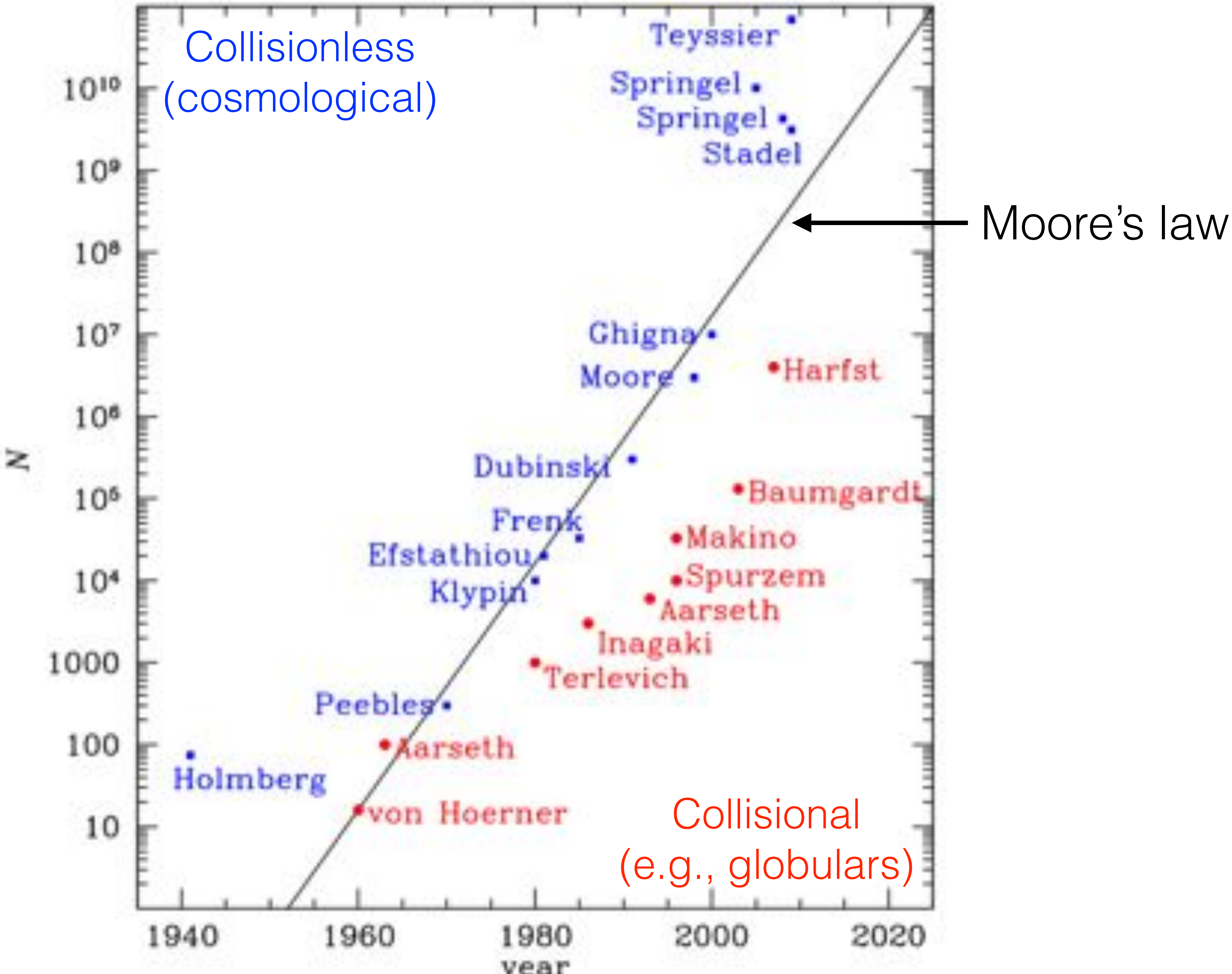

Dehnen & Read 11

Gravity amplifies primordial fluctuations, forms structures

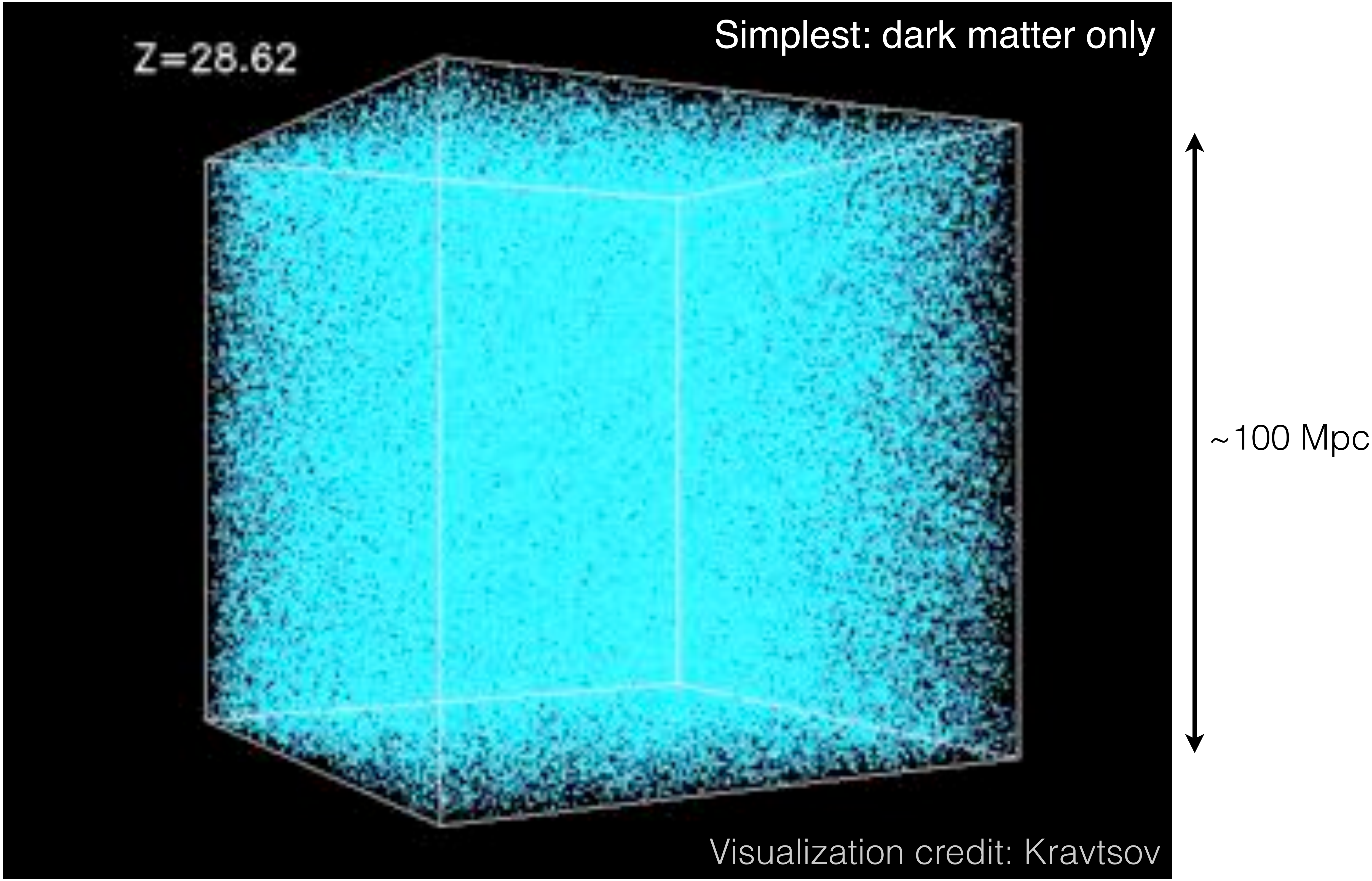

Density peaks (dark matter halos) are the sites of galaxy formation

Millennium simulation

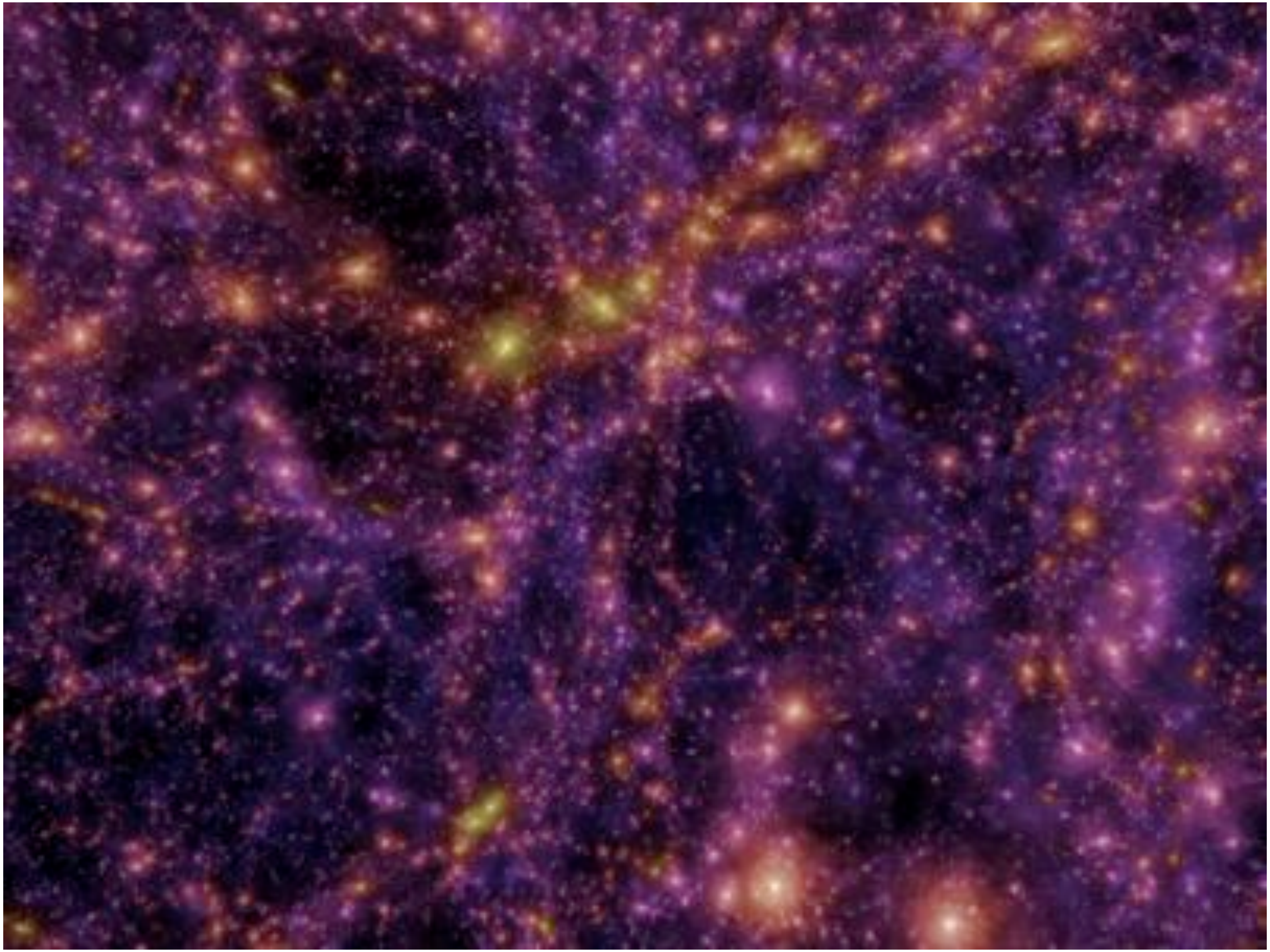

10^{10} particles, 500 h^{-1} Mpc

Springel+05

Dark matter halo mass function

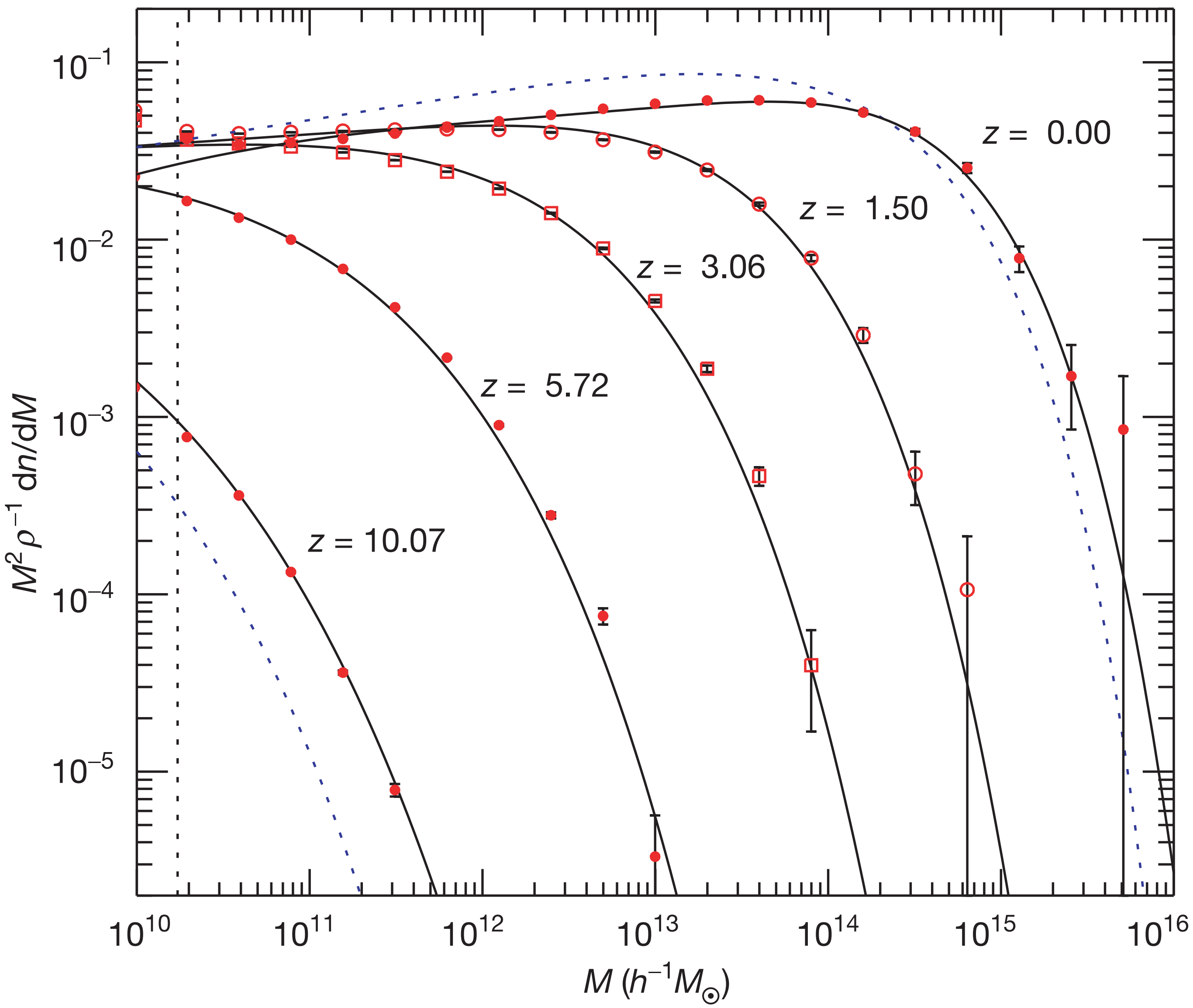

Figure 2 | Differential halo number density as a function of mass and epoch. The function $n(M, z)$ gives the co-moving number density of haloes less massive than M. We plot it as the halo multiplicity function $M^2\rho^{-1}\mathrm{d}n/\mathrm{d}M$ (symbols with 1-σ error bars), where ρ is the mean density of the Universe. Groups of particles were found using a friends-of-friends algorithm[6] with linking length equal to 0.2 of the mean particle separation. The fraction of mass bound to haloes of more than 20 particles (vertical dotted line) grows from 6.42×10^{-4} at $z = 10.07$ to 0.496 at $z = 0$. Solid lines are predictions from an analytic fitting function proposed in previous work[11], and the dashed blue lines give the Press–Schechter model[14] at $z = 10.07$ and $z = 0$.

halos per volume per mass interval

Dimensionless when expressed in terms of 'multiplicity function'

Massive halos $> M_*$

exponentially suppressed (e.g., galaxy clusters today)

MW halo $\approx 10^{12}$ M_{sun}

Press-Schechter is analytic derivation; better fits given by Seth-Tormen function

Springel+05

Dark matter halo mass function

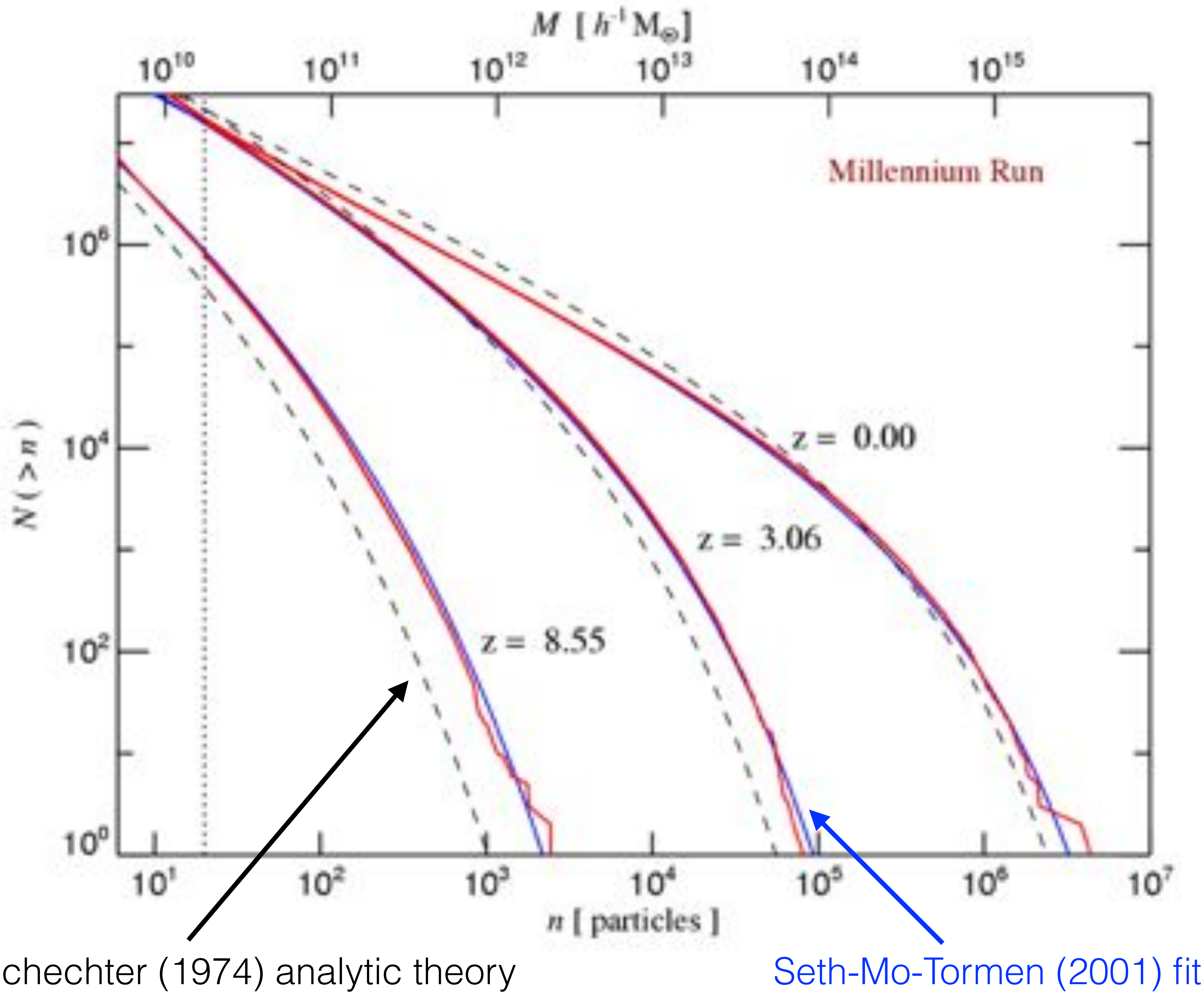

(Nearly) universal dark matter halo profile

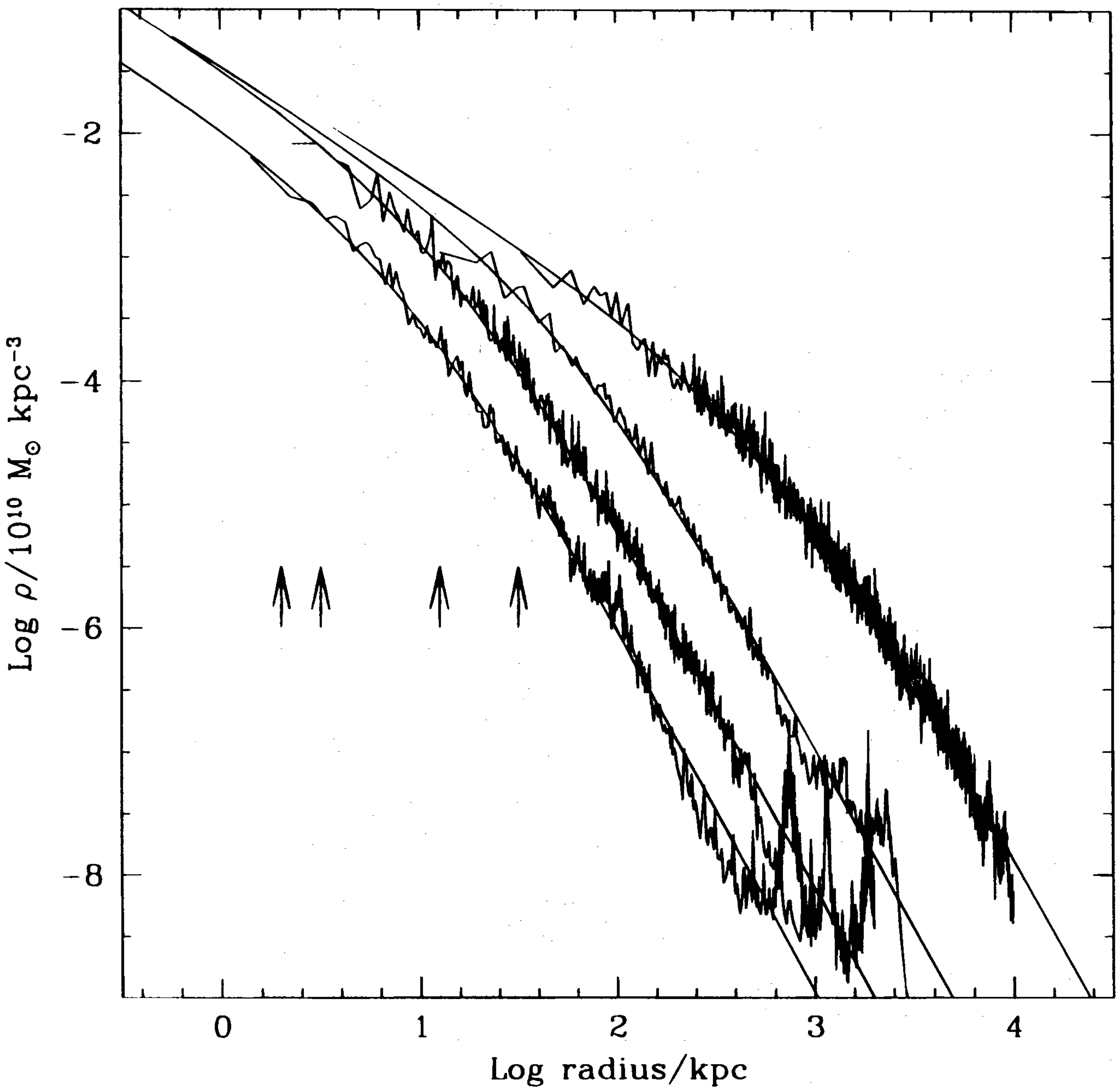

FIG. 3.—Density profiles of four halos spanning 4 orders of magnitude in mass. The arrows indicate the gravitational softening, h_g, of each simulation. Also shown are fits from eq. (3). The fits are good over two decades in radius, approximately from h_g out to the virial radius of each system.

NFW profile

$$\frac{\rho(r)}{\rho_{\rm crit}} = \frac{\delta_c}{(r/r_s)(1 + r/r_s)^2}$$

$$\delta_c = \frac{200}{3} \frac{c^3}{[\ln(1 + c) - c/(1 + c)]}$$

$$r_s = r_{200}/c$$

fits halos of all masses in *N*-body sims

Navarro, Frenk, White 96

Concentration

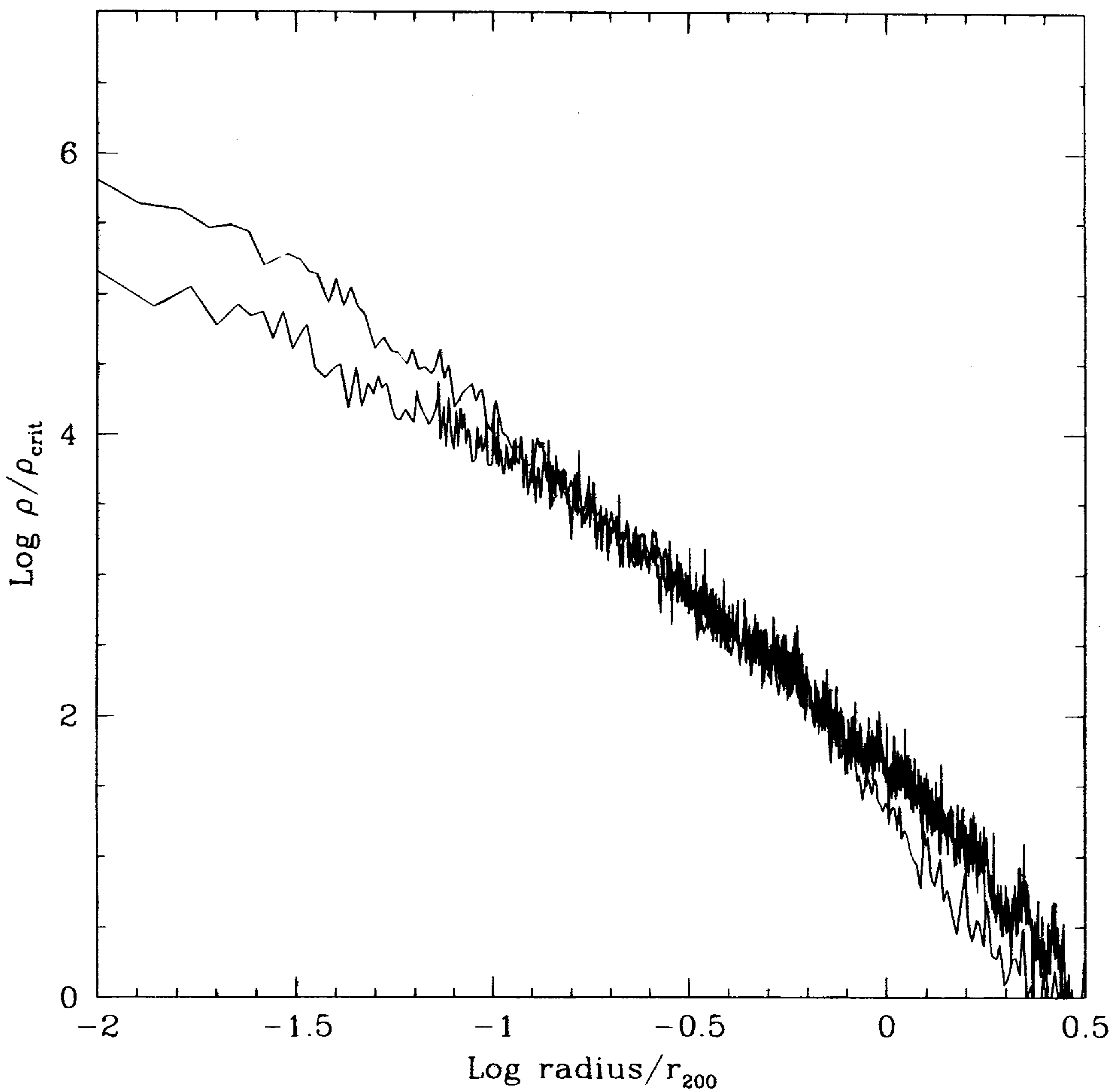

FIG. 4.—Scaled density profiles of the most and least massive halos shown in Fig. 3. The large halo is less centrally concentrated than the less massive system.

At z=0, lower-mass halos are more concentrated

Navarro, Frenk, White 96

Concentration correlates with halo mass

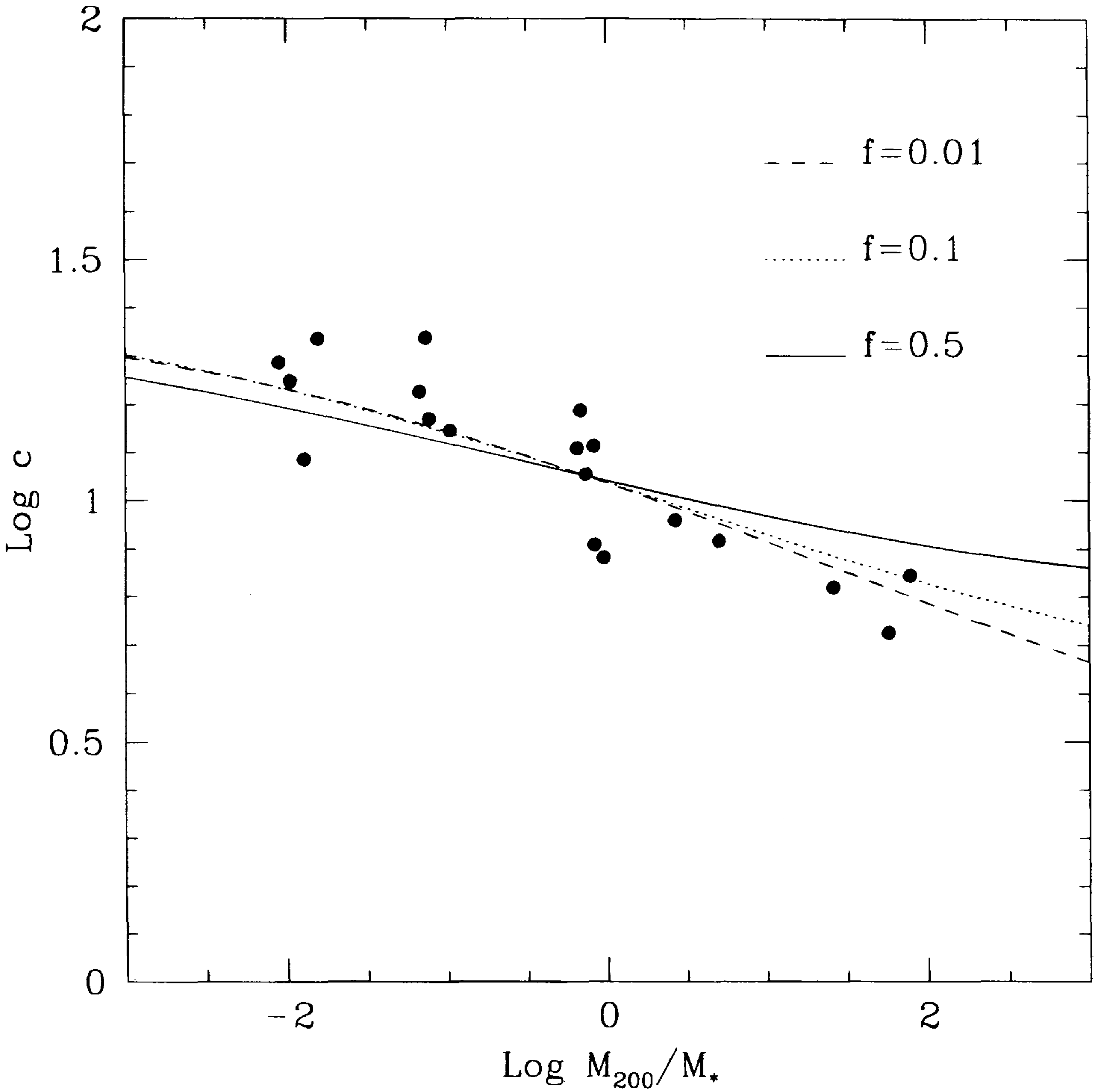

FIG. 8.—Concentration c as a function of the mass of the halo. The curves show the mass-concentration relation predicted from the formation times of halos. All curves are as in Fig. 7 and have been normalized so that they cross at $M_{200} = M_*$.

Dark matter halos profiles form an (approximately) one-parameter family

Parameter is virial mass (equivalently, virial radius)

Seljak 2000: $c = 6\left(\frac{M\mathrm{vir}}{10^{14}h^{-1}\,\mathrm{M}_\odot}\right)^{-1/5}$

Navarro, Frenk, White 96

NFW profile is a generic outcome of CDM models

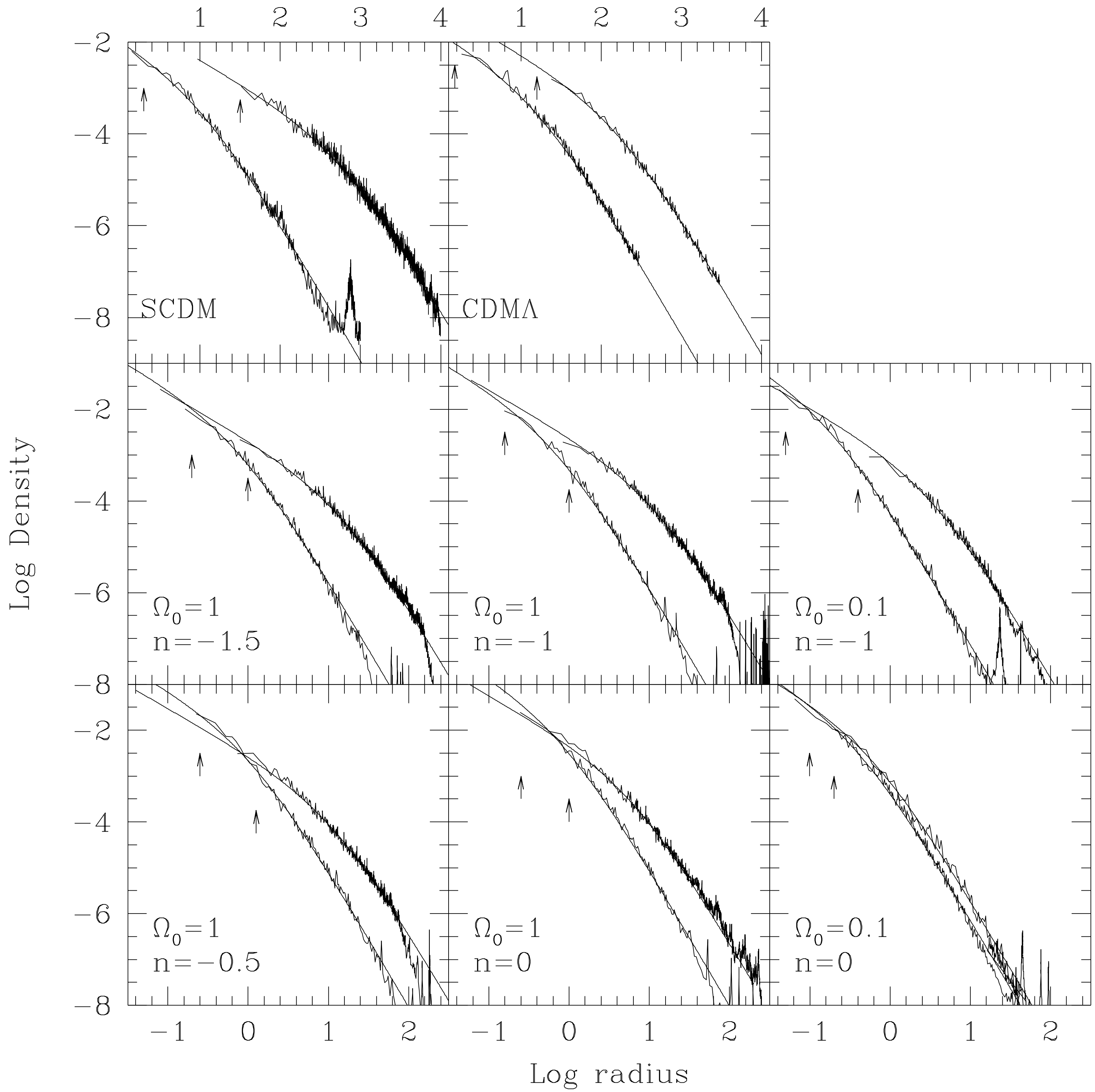

In CDM simulations, NFW profile emerges independent of cosmological parameters (e.g., $\Omega_m \equiv \Omega_0$) and power spectrum of initial conditions (spectral index *n*)

→ attractor solution?

Not well understood, but interesting proposed explanations, e.g. Lithwick & Dalal 11

FIG. 2.—Density profiles of one of the most massive halos and one of the least massive halos in each series. In each panel, the low-mass system is represented by the leftmost curve. In the SCDM and CDMΛ models, radii are given in kiloparsecs (*scale at top*), and densities are in units of $10^{10}\ M_\odot\ \mathrm{kpc}^{-3}$. In all other panels, the units are arbitrary. The density parameter, Ω_0, and the value of the spectral index, *n*, are given in each panel. The solid lines are fits to the density profiles using eq. (1). The arrows indicate the value of the gravitational softening. The virial radius of each system is in all cases 2 orders of magnitude larger than the gravitational softening.

NFW97

Aquarius simulations

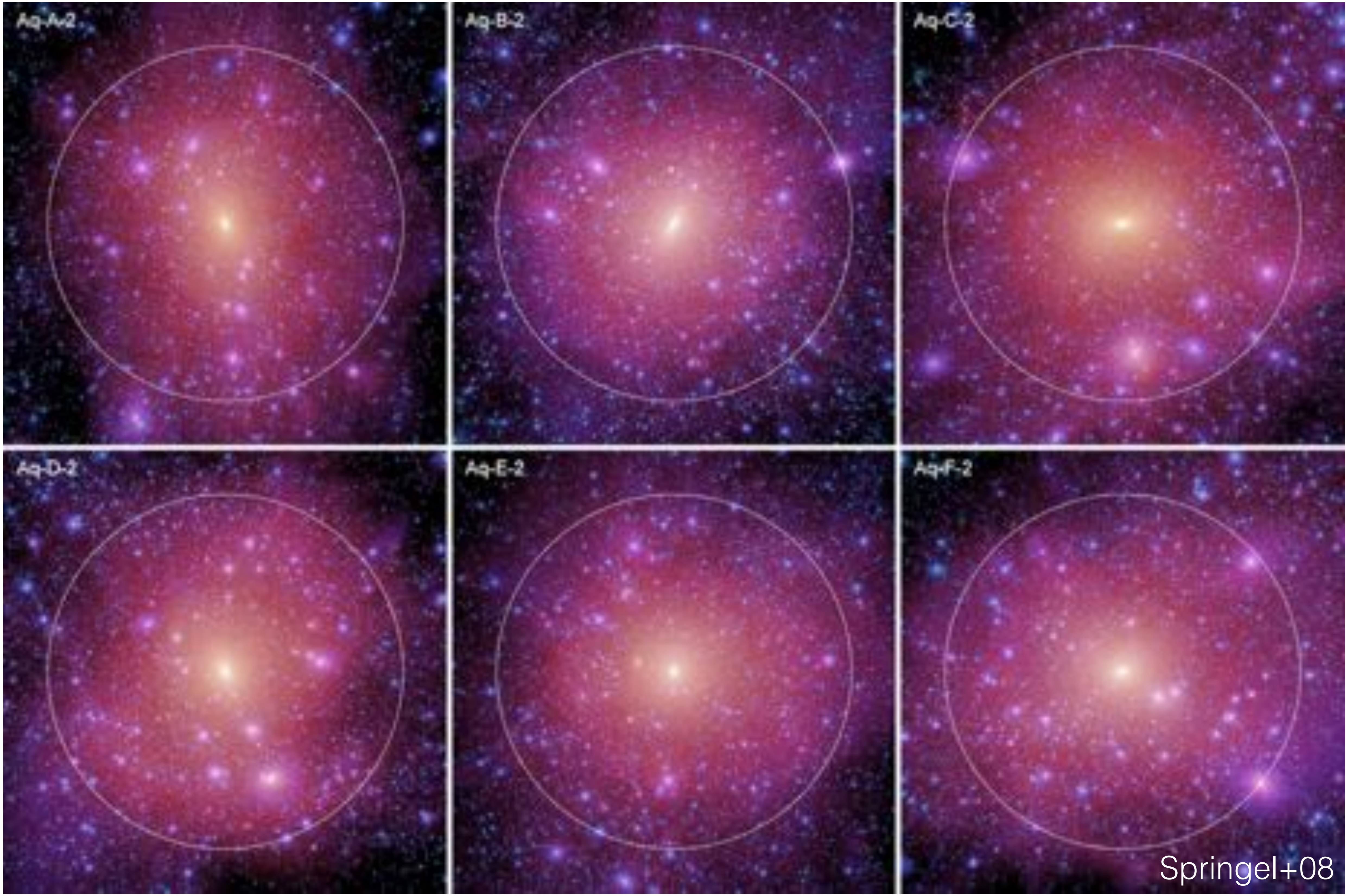

6 $M_{\rm h}$~10^{12} $M_{\rm sun}$ (zoomed in) halos, ultra-high res. (up to 10^9 particles within $R_{\rm vir}$)

Einasto profile $\frac{d\log\rho}{d\log r} = -2\left(\frac{r}{r_{-2}}\right)^{\alpha}$ is better fit at small radius

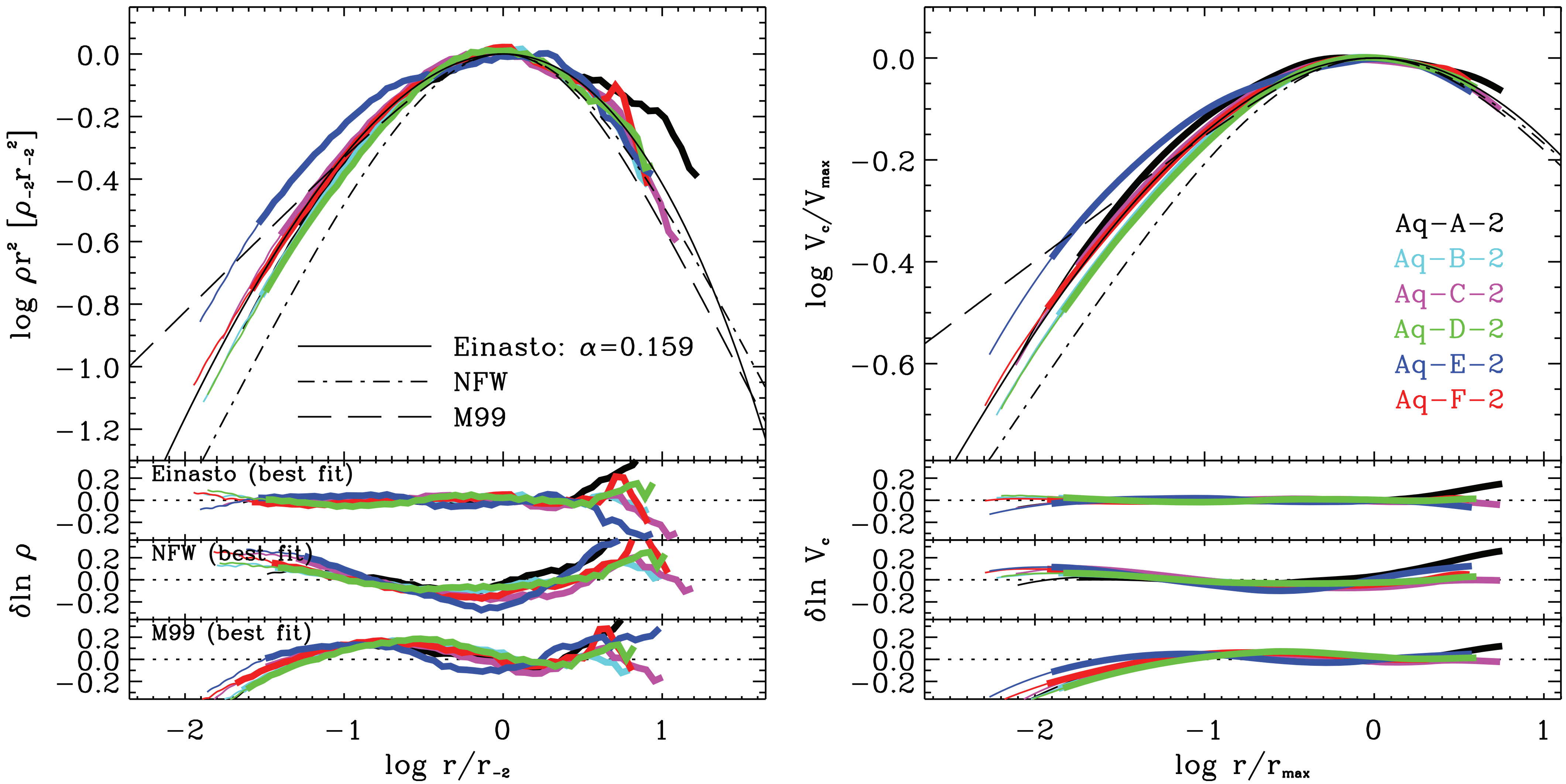

Figure 3. Left-hand panel: spherically averaged density profiles of all level-2 Aquarius haloes. Density estimates have been multiplied by r^2 in order to emphasize details in the comparison. Radii have been scaled to r_{-2}, the radius where the logarithmic slope has the 'isothermal' value, −2. Thick lines show the profiles from $r_{\rm conv}^{(7)}$ outwards; thin lines extend inwards to $r_{\rm conv}^{(1)}$. For comparison, we also show the NFW and M99 profiles, which are fixed in these scaled units. This scaling makes clear that the inner profiles curve inwards more gradually than NFW, and are substantially shallower than predicted by M99. The bottom panels show residuals from the *best fits* (i.e. with the radial scaling free) to the profiles using various fitting formulae (Section 3.2). Note that the Einasto formula fits all profiles well, especially in the inner regions. The shape parameter, α, varies significantly from halo to halo, indicating that the profiles are not strictly self-similar: no simple physical rescaling can match one halo on to another. The NFW formula is also able to reproduce the inner profiles quite well, although the slight mismatch in profile shapes leads to deviations that increase inwards and are maximal at the innermost resolved point. The steeply cusped Moore profile gives the poorest fits. Right-hand panel: same as the left, but for the circular velocity profiles, scaled to match the peak of each profile. This cumulative measure removes the bumps and wiggles induced by substructures and confirms the lack of self-similarity apparent in the left-hand panel.

Note: Einasto is Sérsic with I replace by ρ and R (projected) replaced by r (3D)

Navarro+10

Dark matter substructure

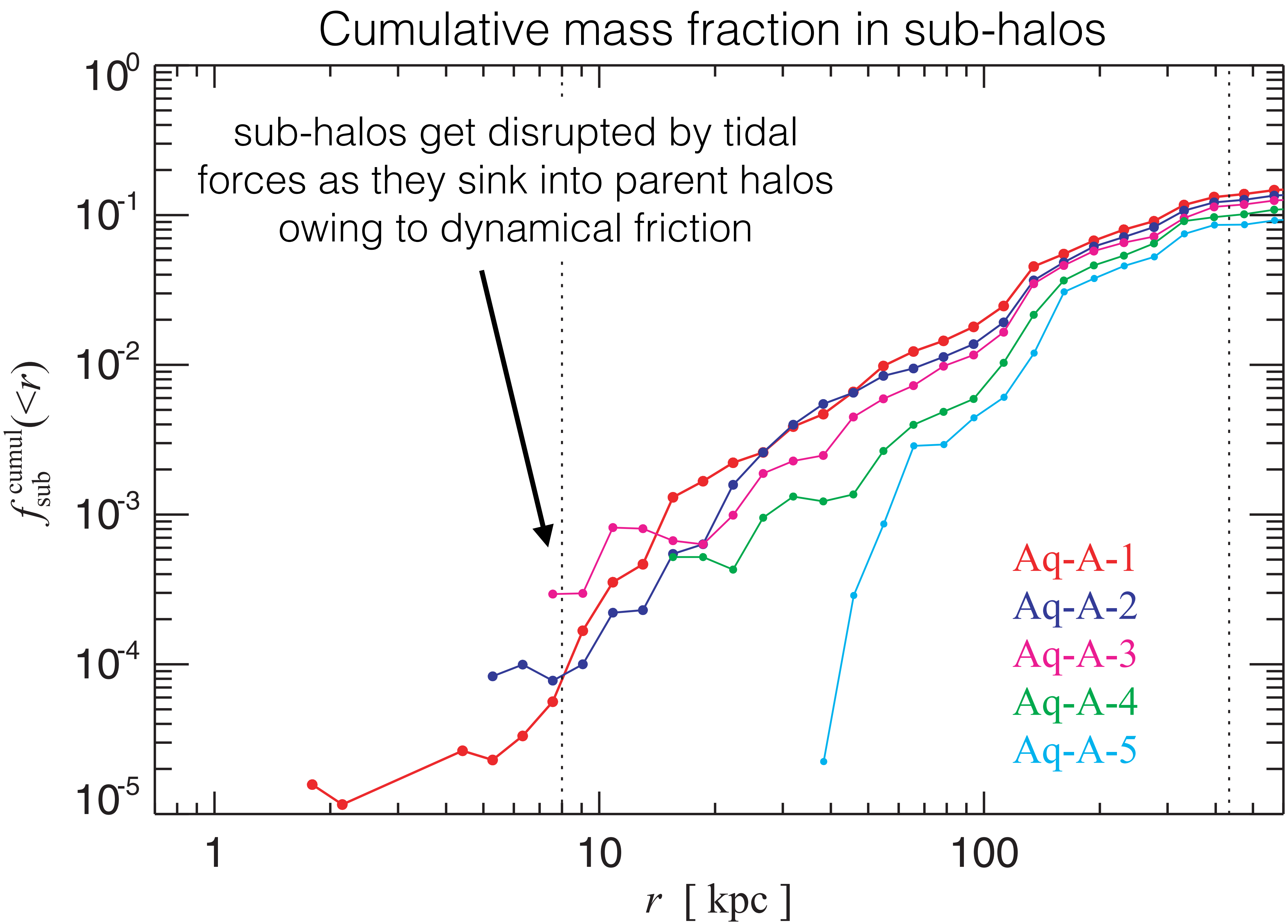

≈10% halo mass in sub-halos

Springel+08

The missing satellites "problem"

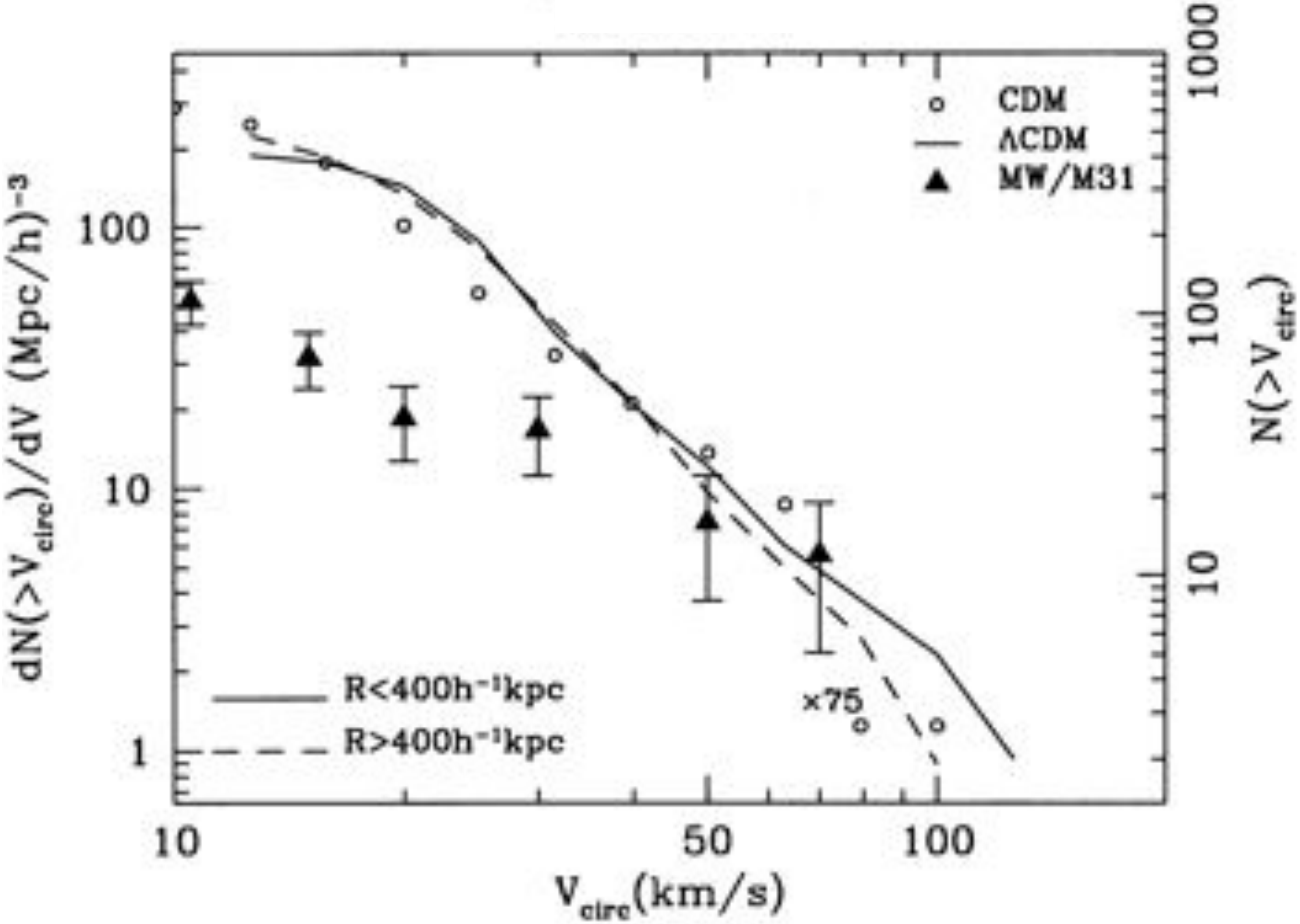

"Cosmological models thus predict that a halo the size of our Galaxy should have about 50 dark matter satellites with circular velocity greater than 20 km s^{-1} and mass greater than 3×10^8 M_{sun} within a 570 kpc radius. This number is significantly higher than the approximately dozen satellites actually observed around our Galaxy." (Klypin+99)

No longer a real "problem": more faint dwarfs now detected, baryonic effects (photoionization, stellar feedback) can suppress dwarf galaxy formation in low-mass halos (e.g., Brooks+12)

Populating halos with galaxies

Three approaches to connect *N*-body simulations to galaxies:

- empirical halo-based models
- semi-analytic models
- hydro simulations

Now comparably successful at producing galaxy populations broadly consistent with observations _but_ different degrees of predictive power _and_ important differences in detail (e.g. mass-metallicity relation)

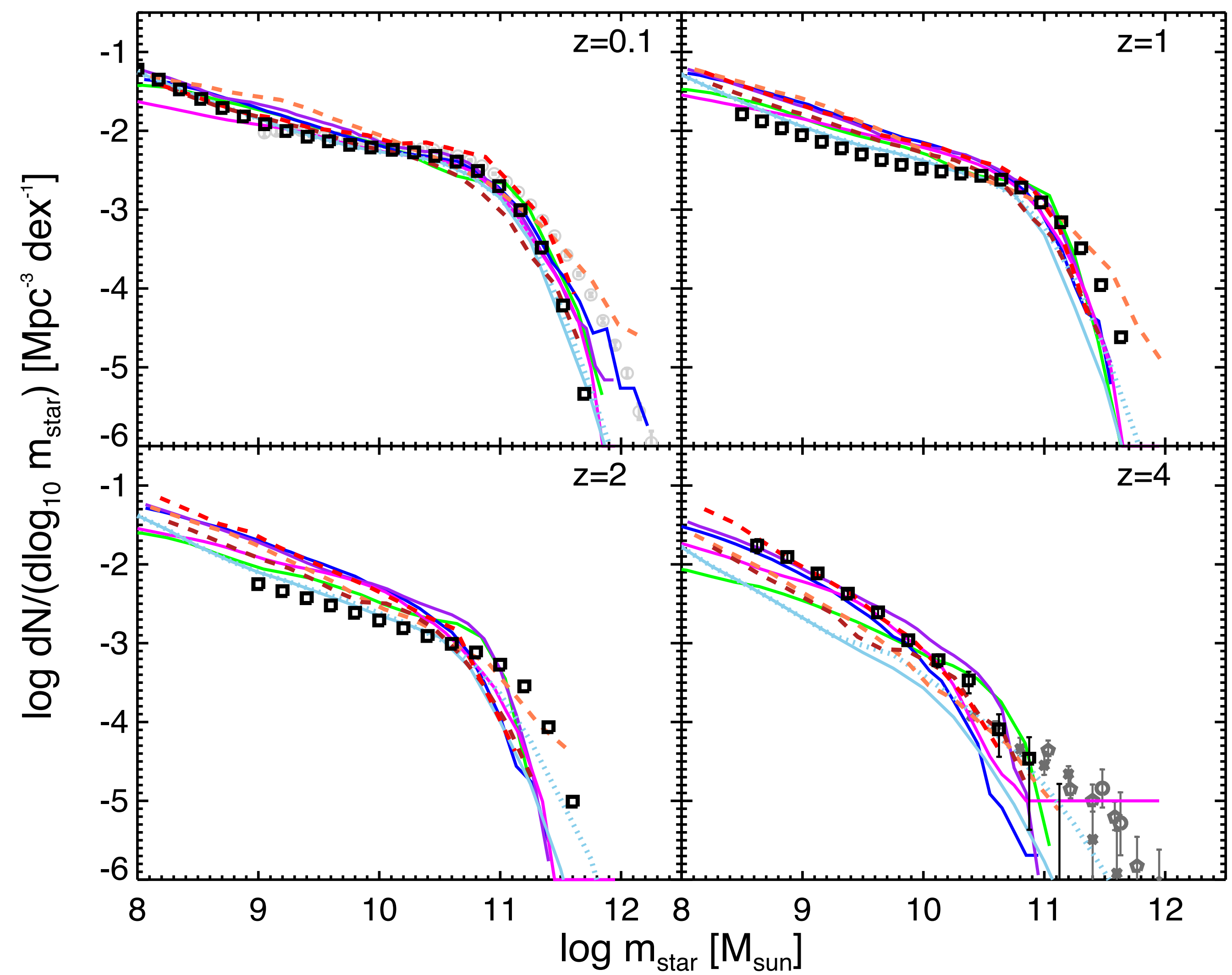

Figure 4:

Galaxy stellar mass function at redshifts $z \sim 0$–4. In the $z = 0.1$, $z = 1$, and $z = 2$ panels, black square symbols show a double-Schechter fit to a compilation of observational estimates. Observations included in the fit are: $z = 0.1$ – Baldry, Glazebrook & Driver (2008), Moustakas et al. (2013); $z = 1$ and $z = 2$ panels – Tomczak et al. (2014), Muzzin et al. (2013). The fits shown at $z = 1$ and $z = 2$ are interpolated to these redshifts from adjacent redshift bins in the original published results. The formal quoted 1σ errors on the estimates shown in these three panels are comparable to the symbol size, and are not shown for clarity (the actual uncertainties are much larger, but are difficult to estimate accurately). In the $z = 0.1$ panel, the estimates of Bernardi et al. (2013) are also shown (open gray circles). In the $z = 4$ panel we show estimates from Duncan et al. (2014, triangles), Caputi et al. (2011, crosses), Marchesini et al. (2010, circles, for $z = 3$–4), and Muzzin et al. (2013, pentagons, $z = 3$–4). Solid colored lines show predictions from semi-analytic models: SAGE (Croton et al. in prep, dark blue), Y. Lu SAM (Lu et al. 2013, magenta), GALFORM (Gonzalez-Perez et al. 2014, green), the Santa Cruz SAM (Porter et al. 2014, purple), and the MPA Millennium SAM (Henriques et al. 2013). The dotted light blue line shows the Henriques et al. (2013) SAM with observational errors convolved (see text). Colored dashed lines show predictions from numerical hydrodynamic simulations: EAGLE simulations (Schaye et al. 2014, dark red), ezw simulations of Davé and collaborators (Davé et al. 2013, bright red) and the Illustris simulations (Vogelsberger et al. 2014b, orange).

Somerville & Davé review, in prep.

Abundance matching

Assume monotonic relationship between stellar mass and dark matter halo mass, i.e.

in given volume, highest stellar mass is assigned to most massive dark halo, …

Comparison of stellar mass and dark matter halo mass functions yields $M_\bigstar/M_{\rm halo}$ relationship

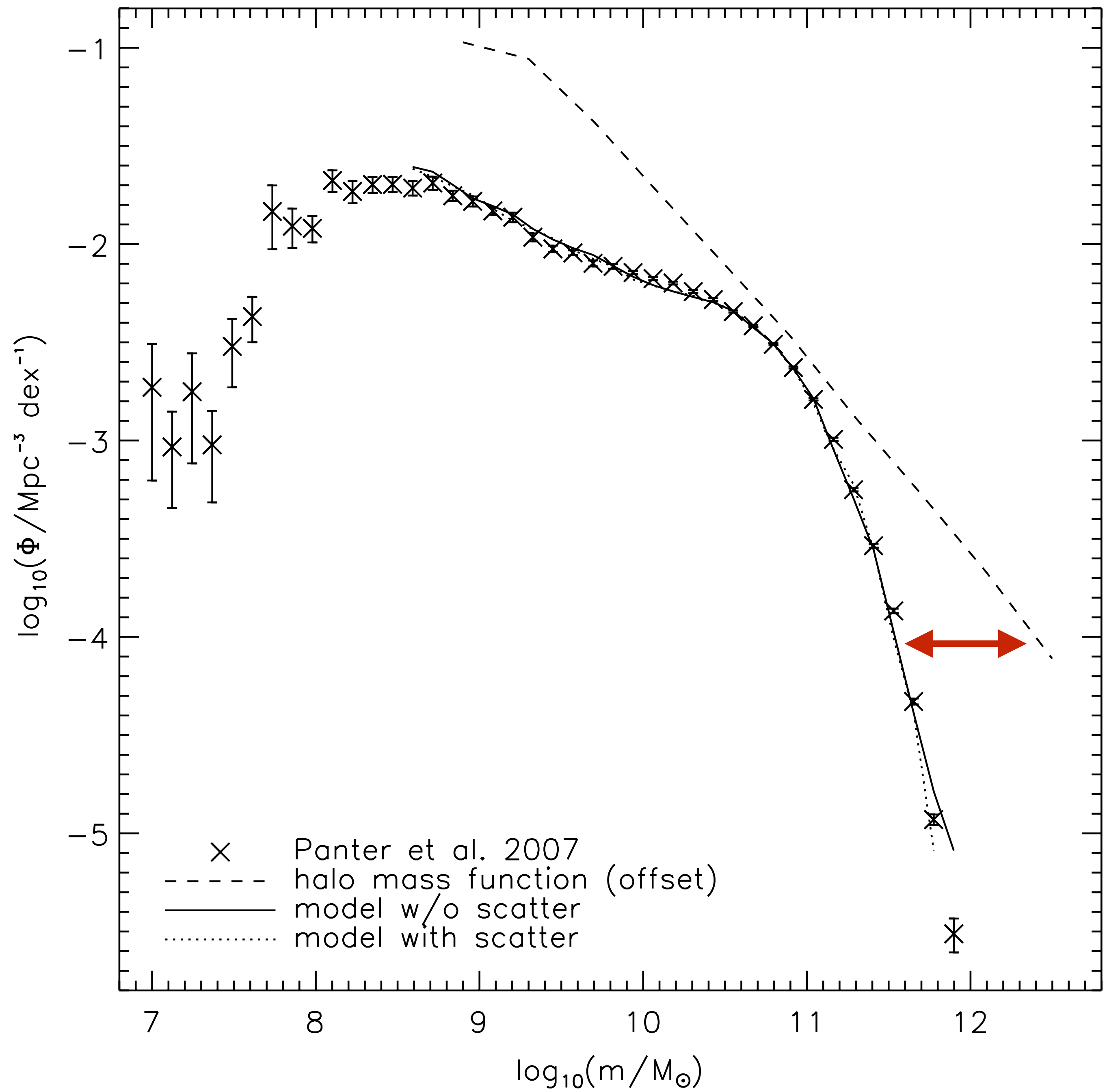

Figure 1. Comparison between the halo mass function offset by a factor of 0.05 (dashed line), the observed galaxy mass function (symbols), our model without scatter (solid line), and our model including scatter (dotted line).We see that the halo and the galaxy mass functions are different shapes, implying that the stellar-to-halo mass ratio m/M is not constant. Our four-parameter model for the halo mass dependent stellar-to-halo mass ratio is in very good agreement with the observations (both including and neglecting scatter).

Moster+10

Abundance matching result at z=0

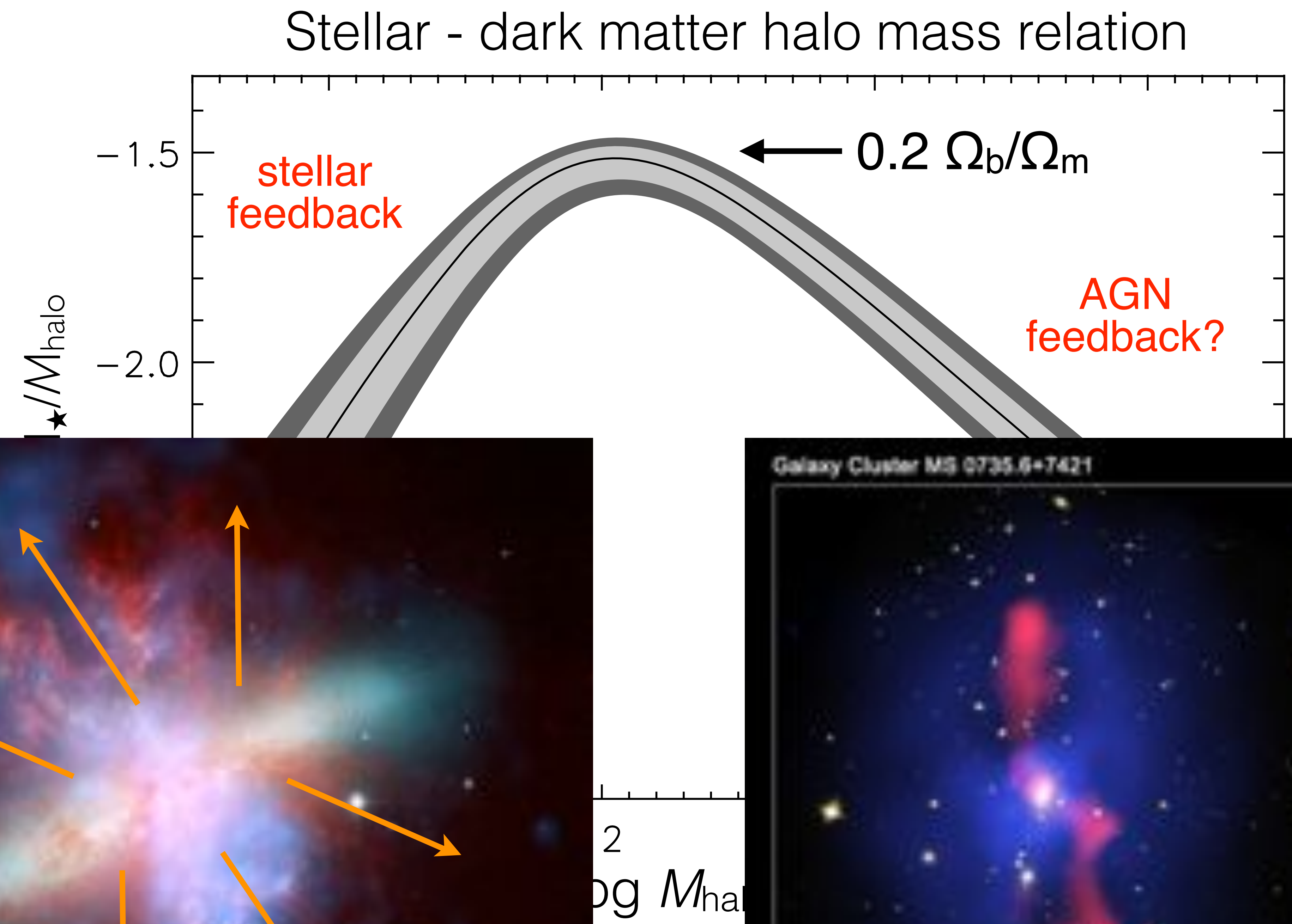

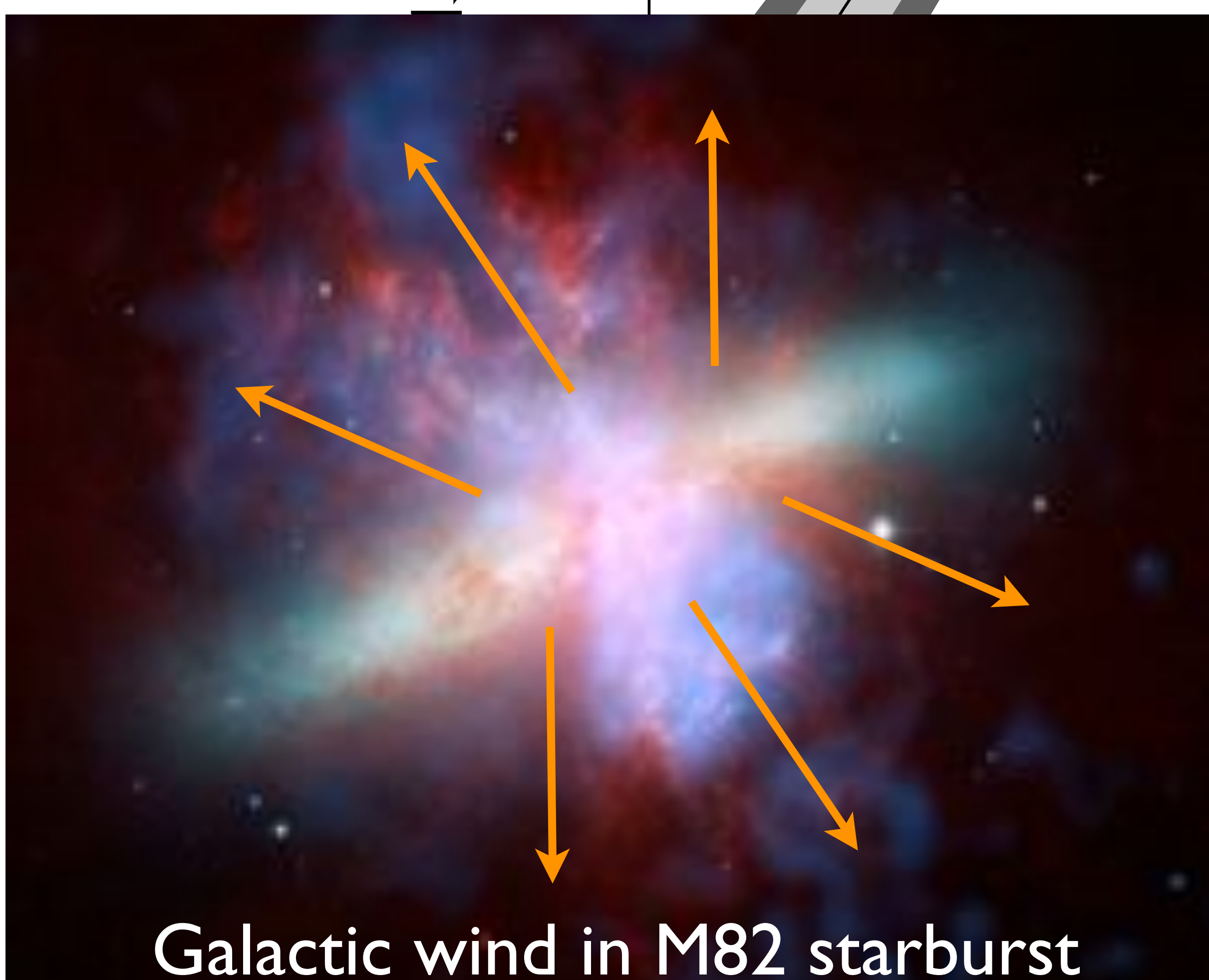

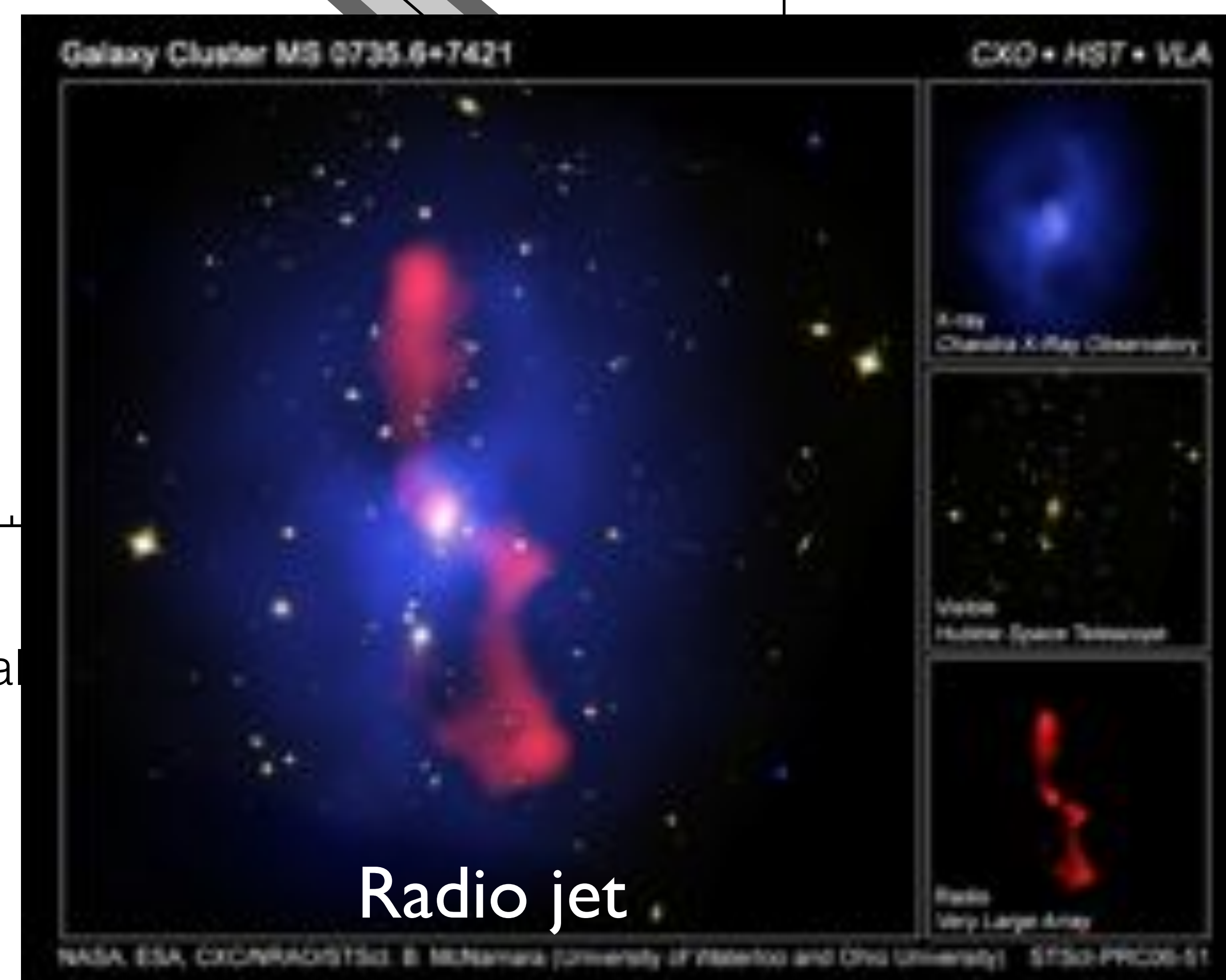

Semi-analytic models (SAMs)

Assume galaxies form inside dark matter halos → merger trees

Use simple analytic models ('recipes') to determine galaxy properties
- gas cooling
- angular momentum of disk
- effects of feedback, …

Analytic prescriptions do not capture full complexity of galaxy formation, so parameters are tuned to match observations

Computationally inexpensive, so can systematically explore parameter space

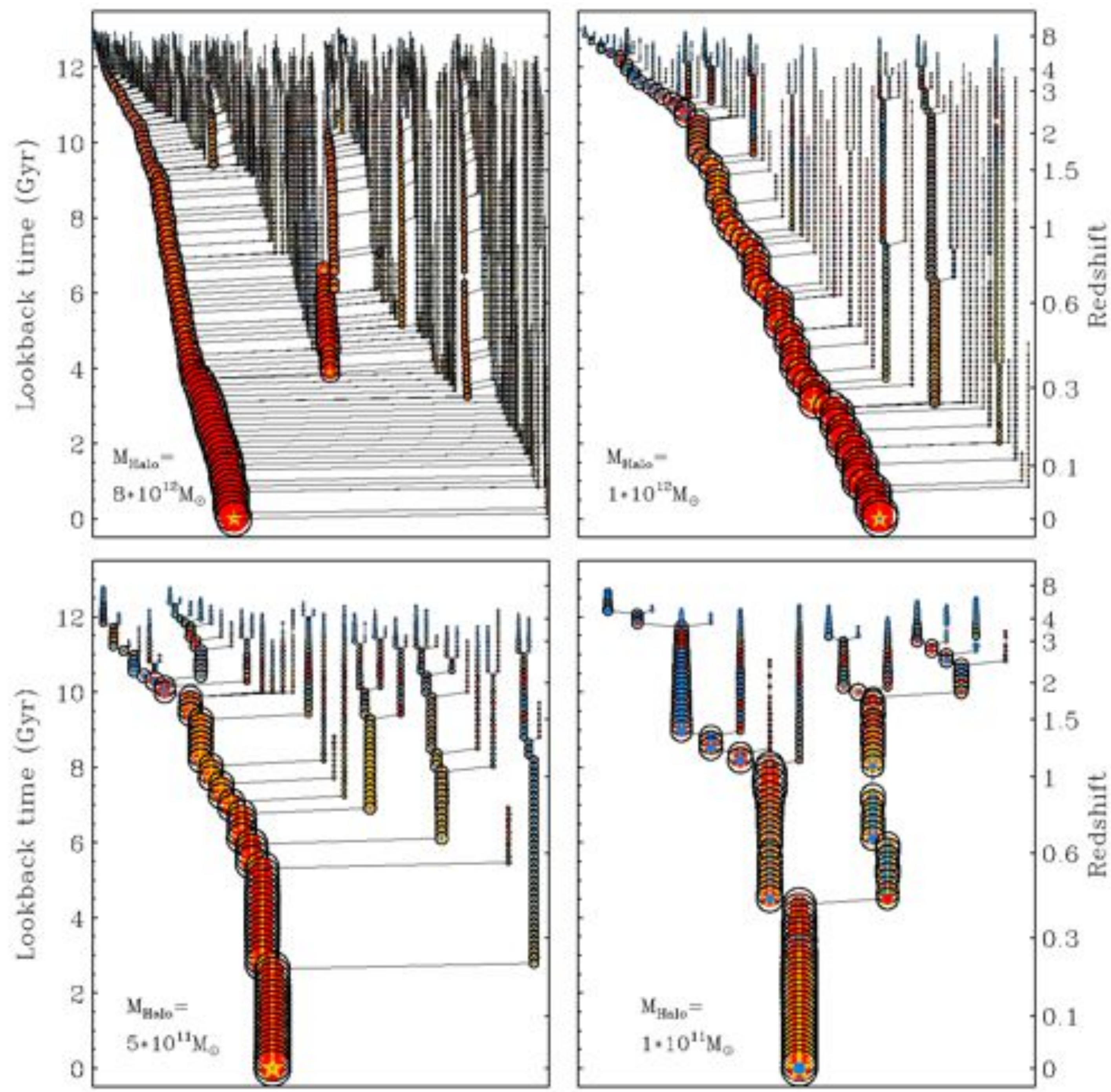

Figure 3:

Visualization of representative predictions from a semi-analytic model. Symbol sizes represent the mass of the host dark matter halo; the x-axis is arbitrary. Symbols connected by lines represent halo mergers. Colors represent the mass of different galaxy components (red: hot gas; blue: cold gas; yellow: stars). Several different final host halo masses are shown as indicated on the figure panels. Reproduced from Hirschmann et al. (2012a).

Somerville & Davé review, in prep.

Hydrodynamical simulations of galaxy formation

Explicitly include baryons in the simulation and attempt to explicitly capture all important physics

Limited by computational power, so still need to rely on ‘sub-resolution models’ for processes occurring below resolution limit (e.g., star formation)

Large-volume (~100 Mpc) hydro sims have typical resolution ~1 kpc; zoom-ins ~10 pc

Most detailed predictions, e.g. gas around galaxies (the circum-galactic and intergalactic media)

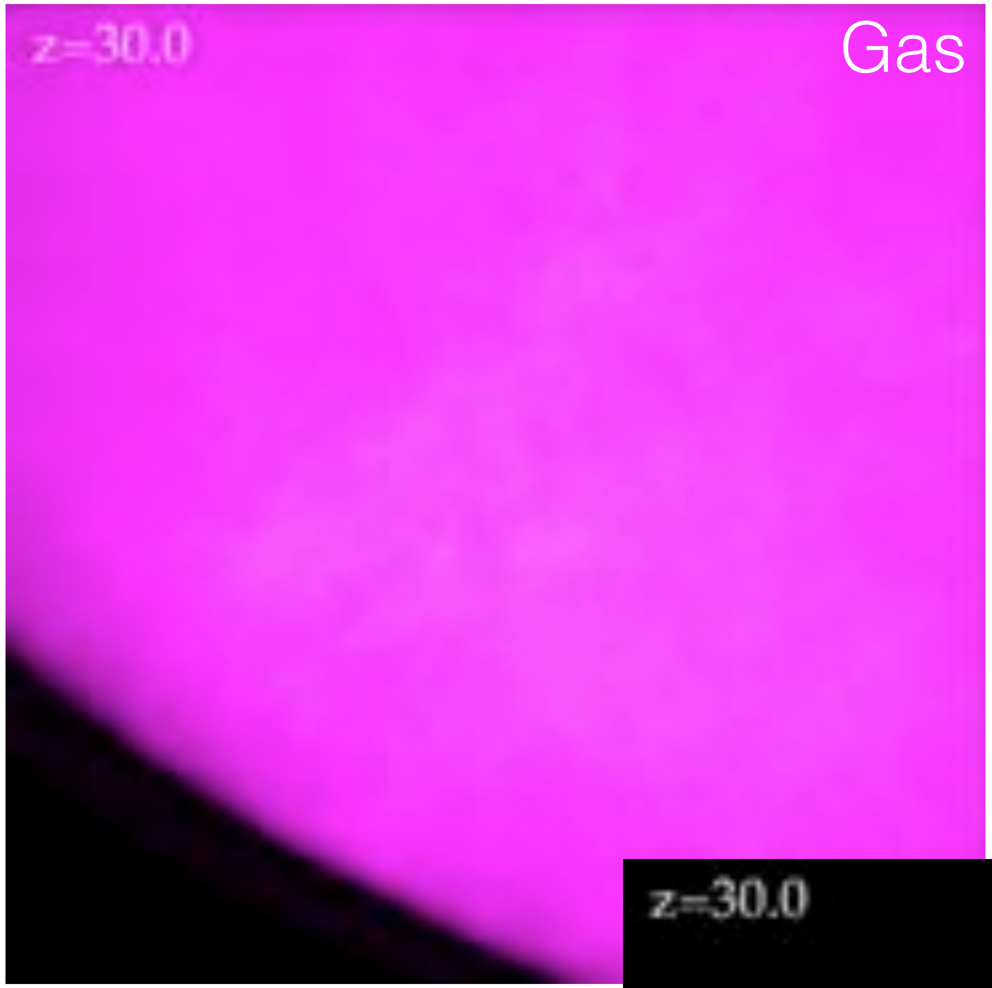

Movie of FIRE zoom-in of MW-like galaxy

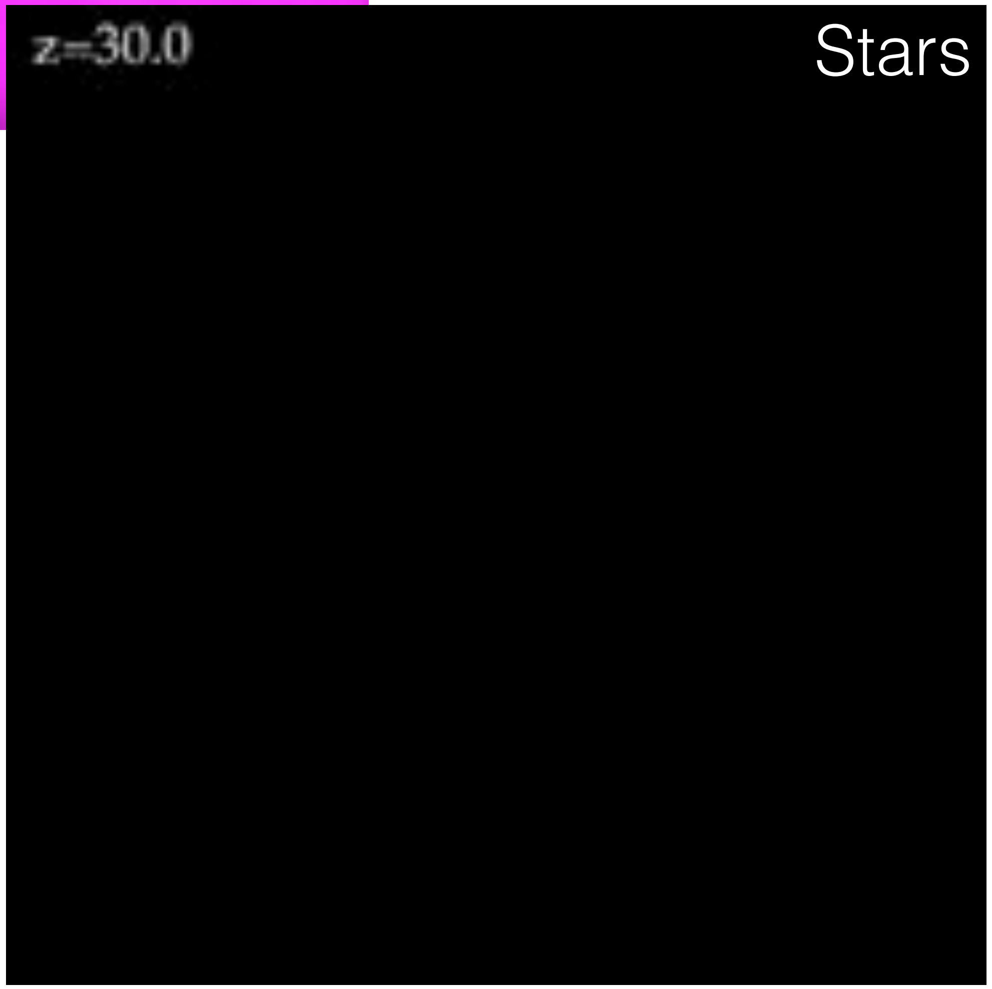

Galaxy clustering

When populated with galaxies, the cosmic web of dark matter predicted by cosmological N-body simulations explains the observed clustering of galaxies

→ strong evidence in support of gravitational instability-induced large-scale structure as predicted by ΛCDM

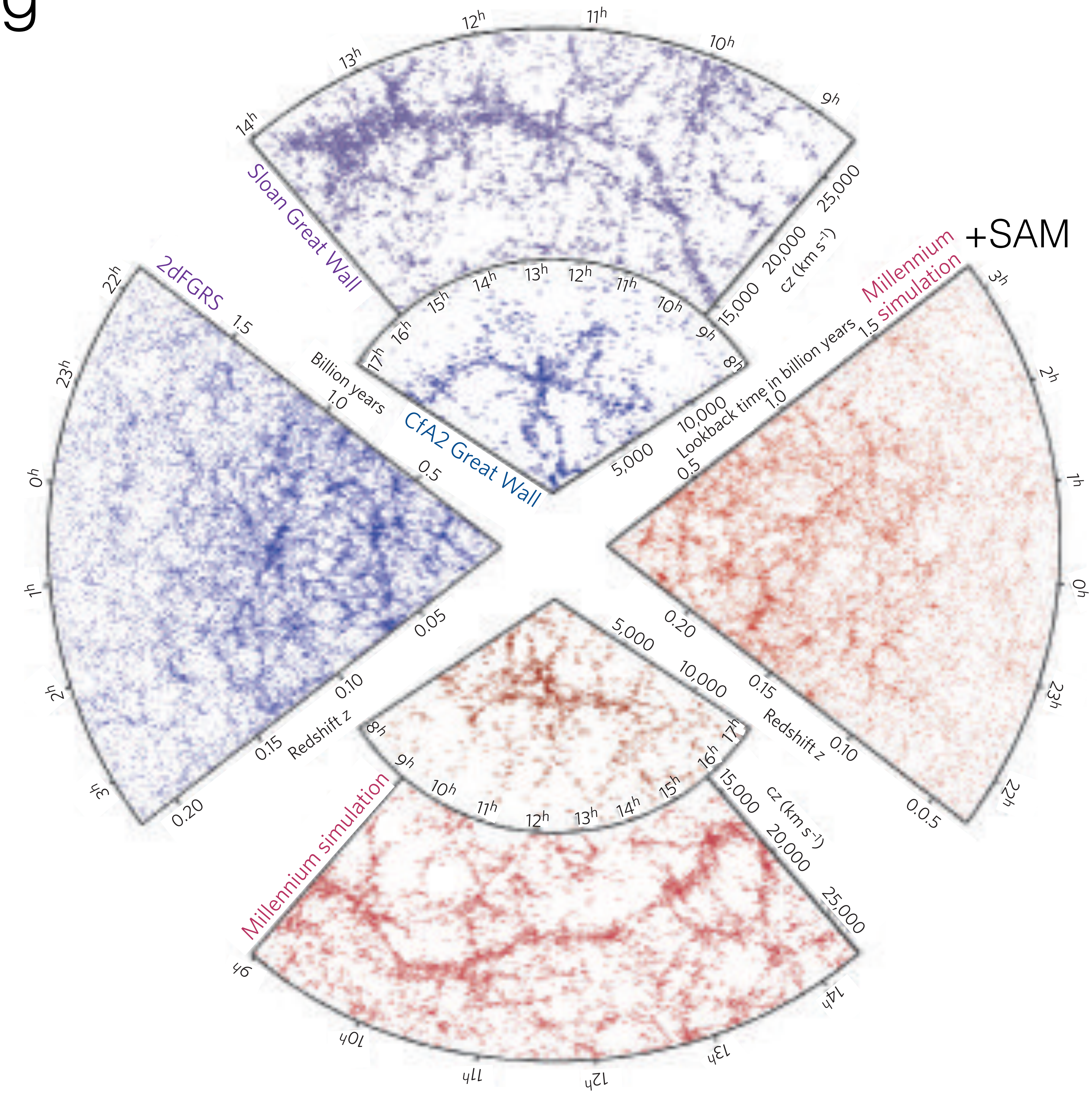

Springel, Frenk, White 06

Correlations functions

Clustering is made quantitative using correlation functions

$$dP = n[1 + \xi(r)]dV$$

which quantify the 'excess probability' of finding a galaxy (or halo) close to another one

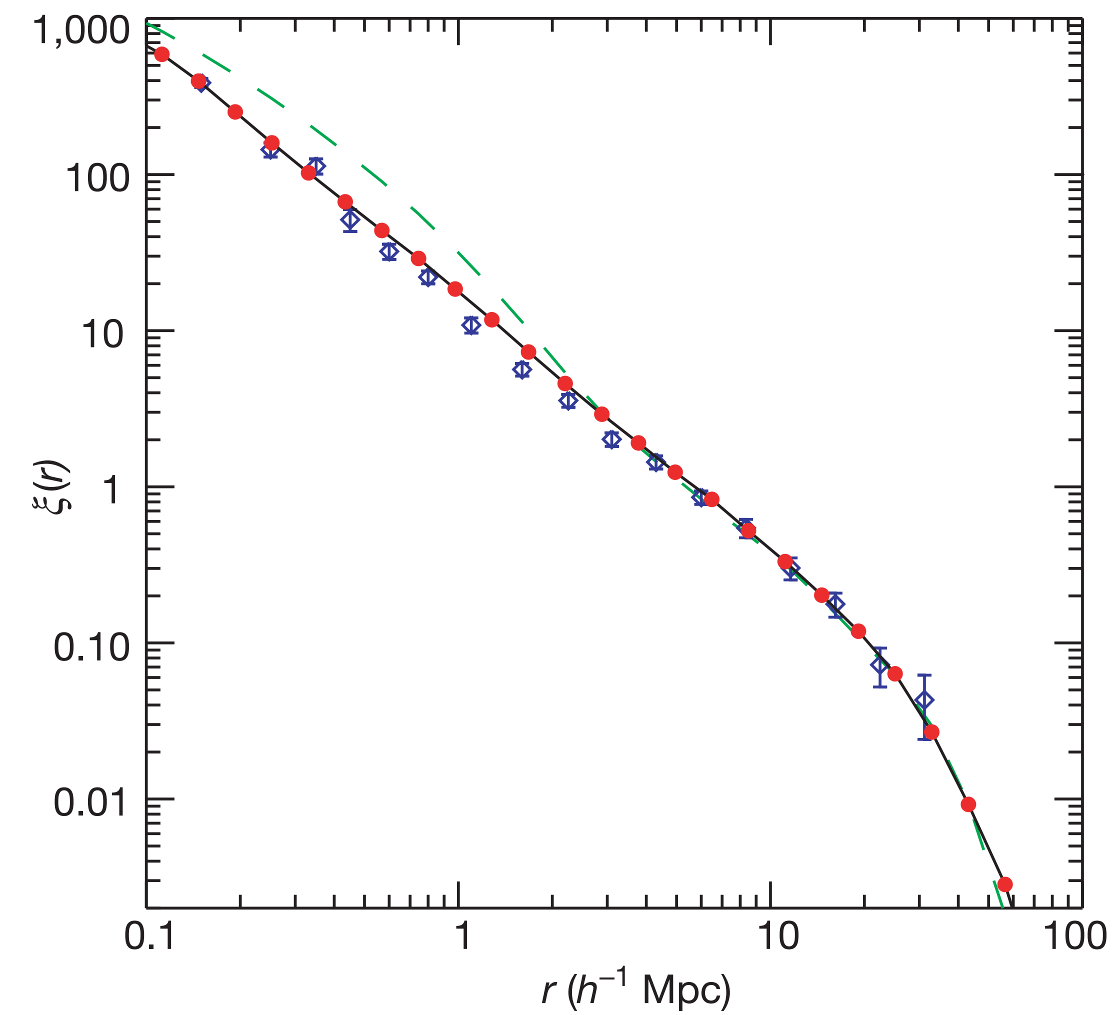

Figure 4 | Galaxy two-point correlation function, $\xi(r)$, at the present epoch as a function of separation r. Red symbols (with vanishingly small Poisson error bars) show measurements for model galaxies brighter than $M_K = -23$, where M_K is the magnitude in the K-band. Data for the large spectroscopic redshift survey 2dFGRS (ref. 28) are shown as blue diamonds together with their 1-σ error bars. The SDSS (ref. 34) and APM (ref. 31) surveys give similar results. Both for the observational data and for the simulated galaxies, the correlation function is very close to a power law for $r \leq 20h^{-1}$ Mpc. By contrast, the correlation function for the dark matter (dashed green line) deviates strongly from a power law.

Springel+05

N-body algorithms

Barnes-Hut tree

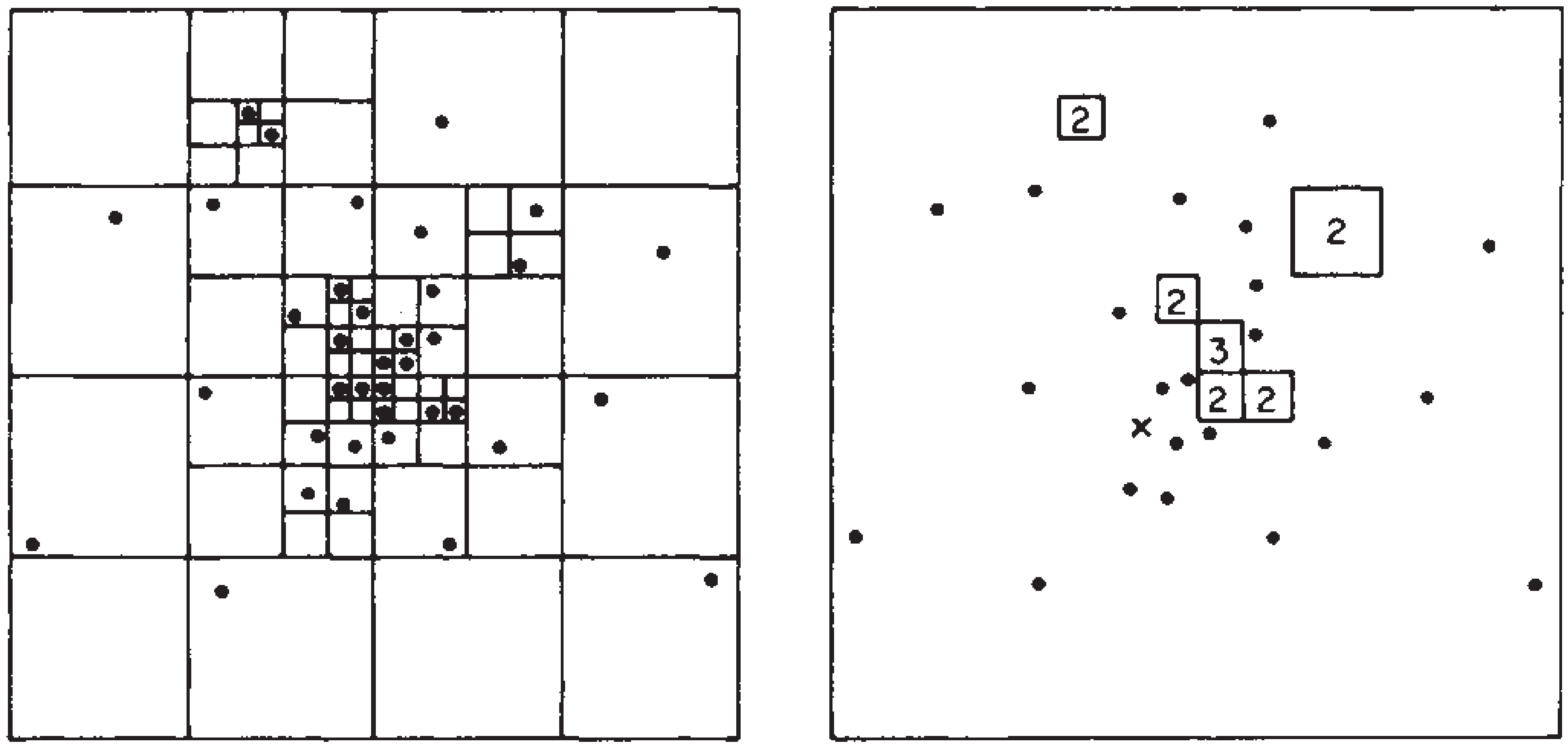

Fig. 1 Hierarchical boxing and force calculation, presented for simplicity in two dimensions. On the left, a system of particles and the recursive subdivision of system space induced by these particles. Our algorithm makes the minimum number of subdivisions necessary to isolate each particle. On the right, how the force on particle *x* is calculated. Fitted cells contain particles that have been lumped together by our 'opening angle' criterion; each such cell represents a single term in the force summation.

Barnes & Hut 86

Barnes-Hut tree

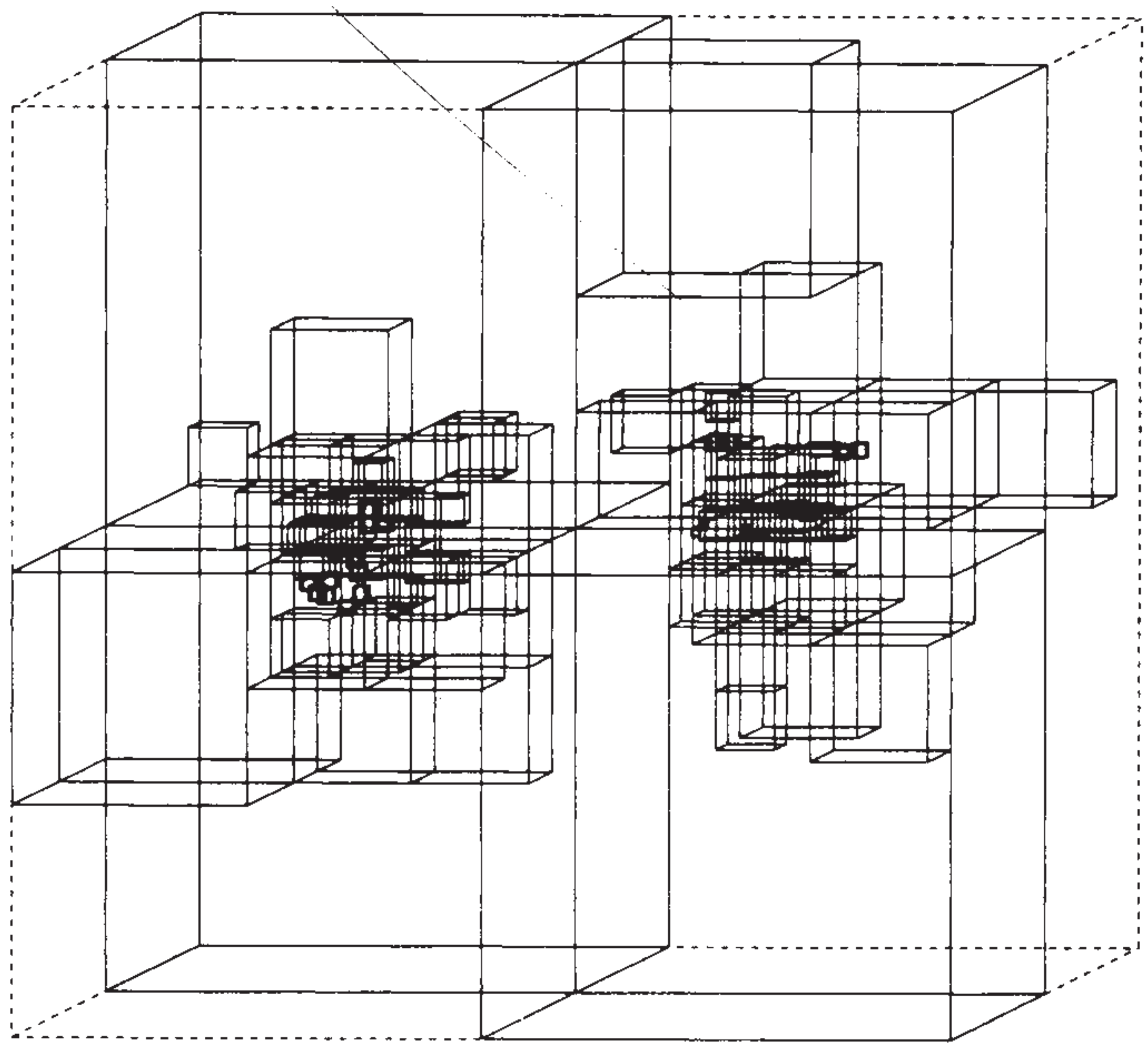

Fig. 2 Box structure induced by a three-dimensional particle distribution. This example was taken from the early stages of an encounter of two $N = 64$ systems, and shows how the boxing algorithm can accommodate systems with arbitrarily complicated geometry. The particle distribution corresponding to a system with 32 times as many members is shown in Fig. 3.

Barnes & Hut 86

Adaptive mesh refinement

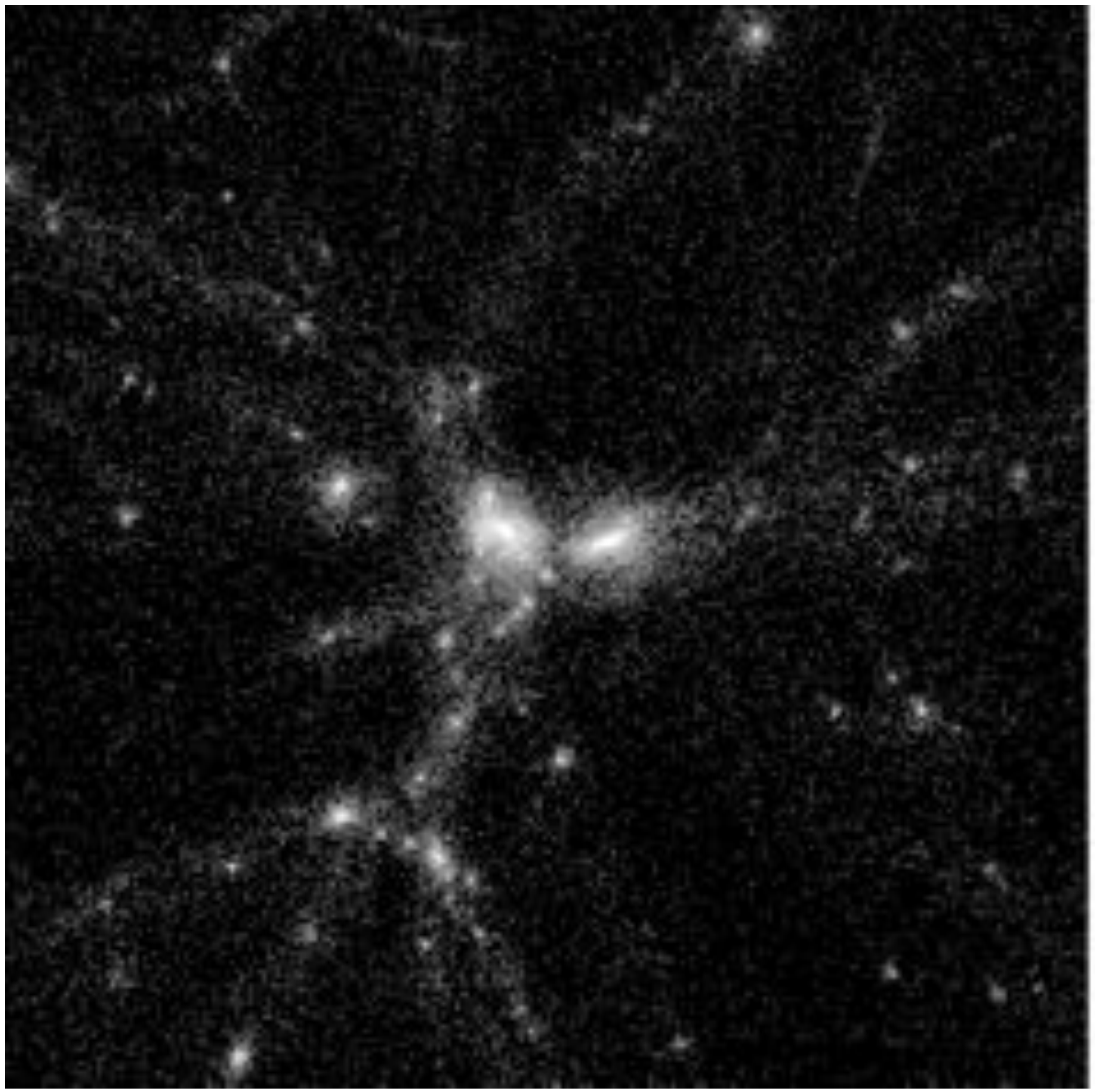

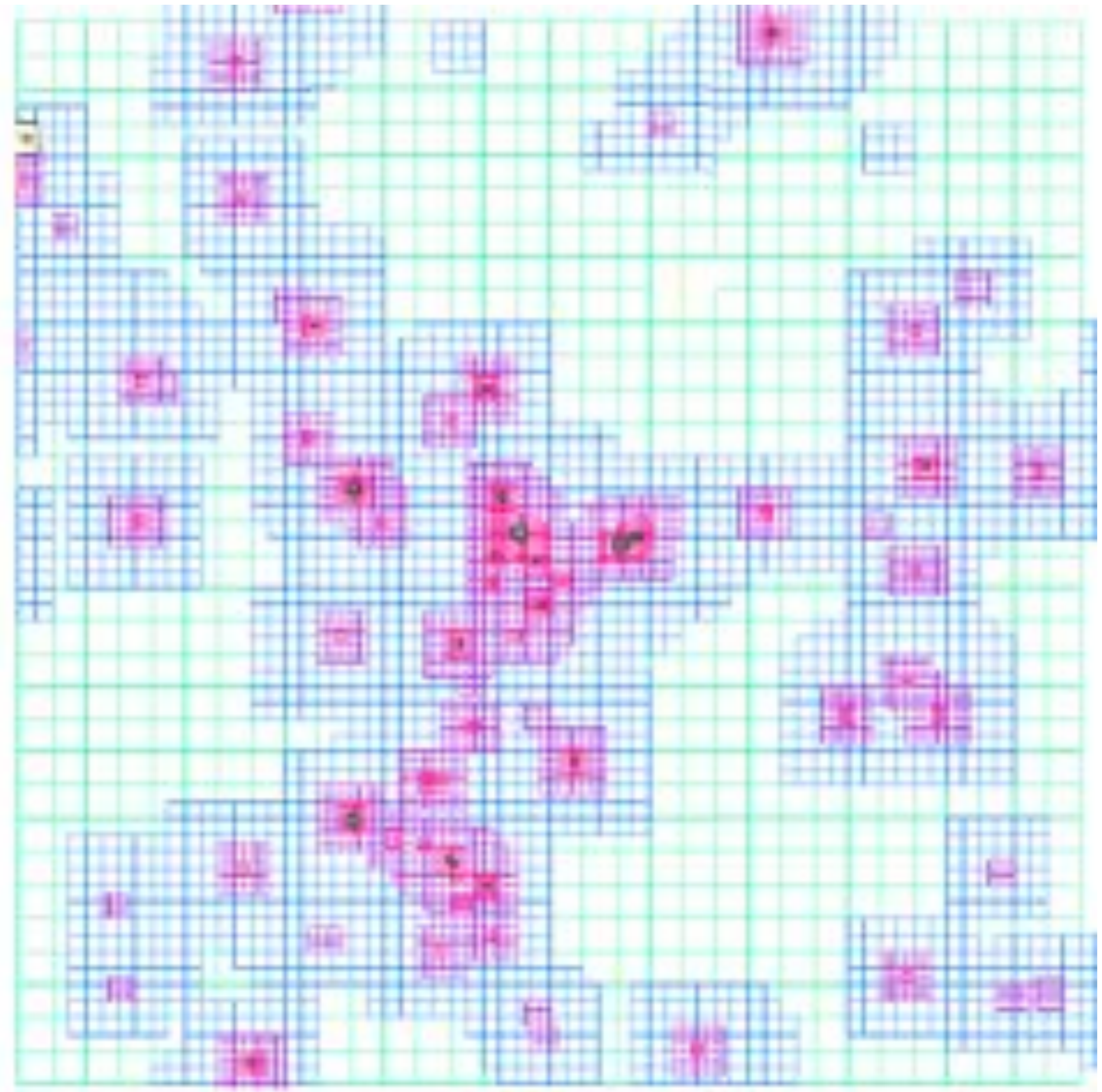

Generally not as accurate at tree codes for gravity but useful because hydro often solved on a grid, too.

Modern gravity solvers vs. direct summation

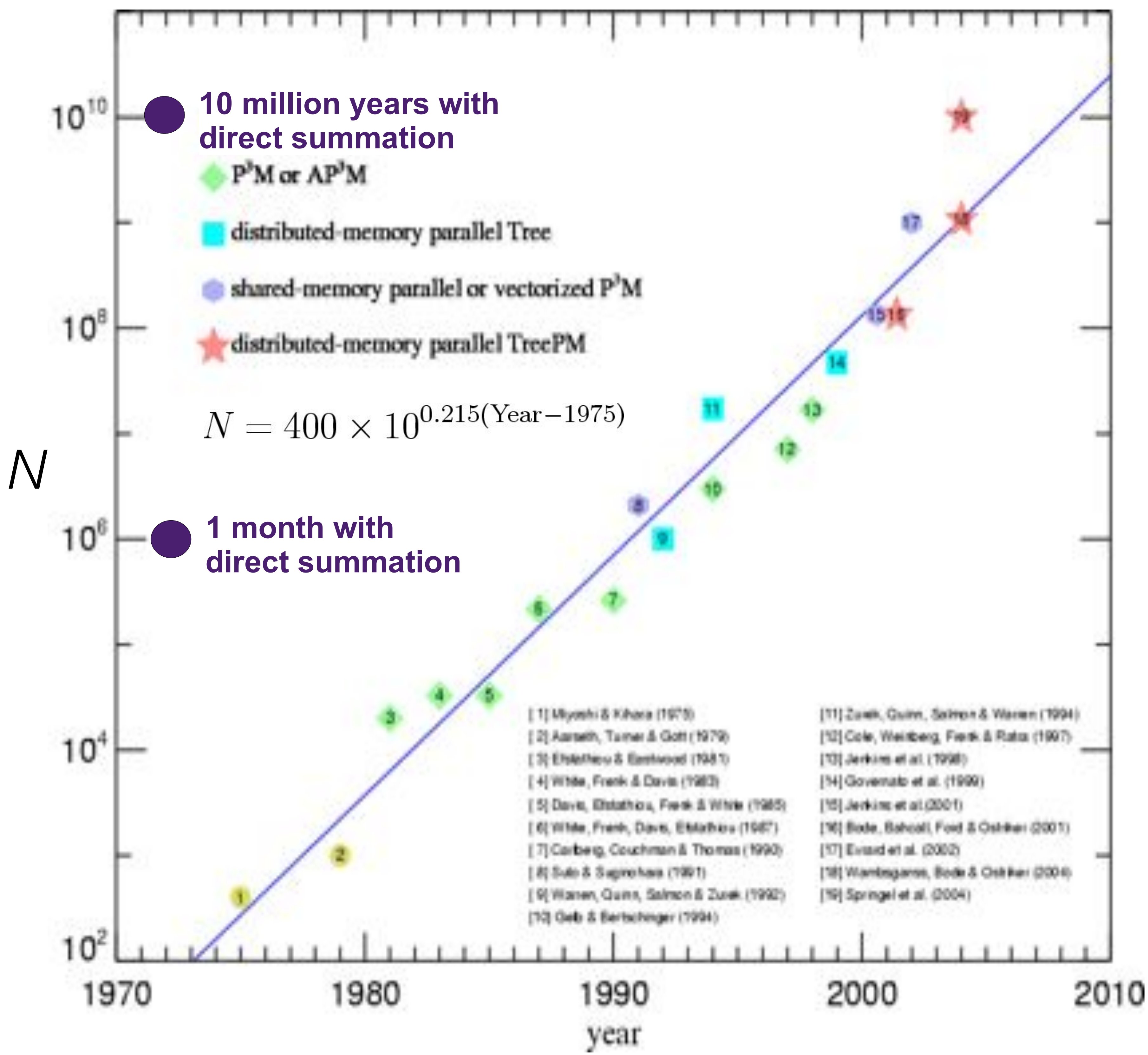

Springel

Hydro solvers

Eulerian

discretize space

representation on a mesh
(volume elements)

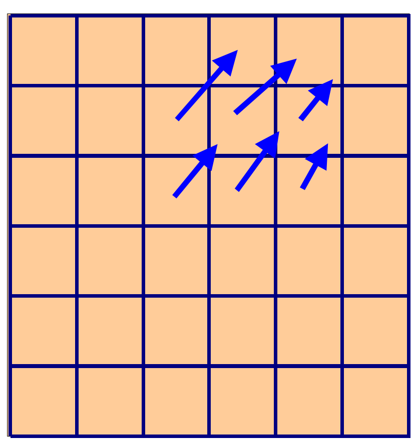

principle advantage:

high accuracy (shock capturing), low numerical viscosity

grid-based Godunov schemes

Athena, ENZO, RAMSES, …

Lagrangian

discretize mass

representation by fluid elements
(particles)

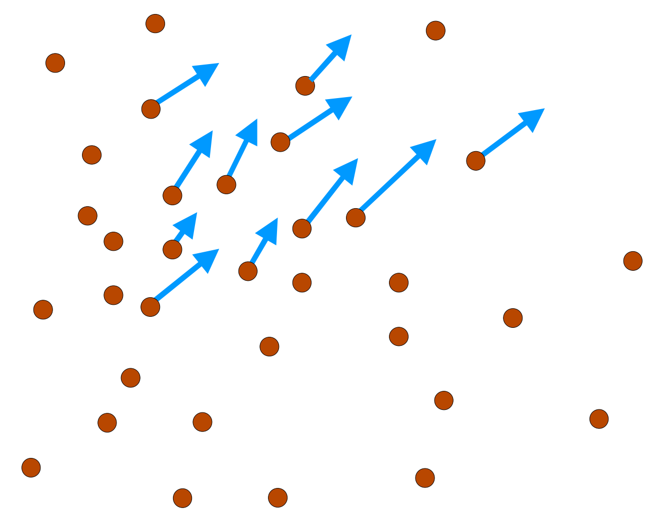

principle advantage:

resolutions adjusts automatically to the flow

e.g., smooth particle hydrodynamics

GADGET, Gasoline…

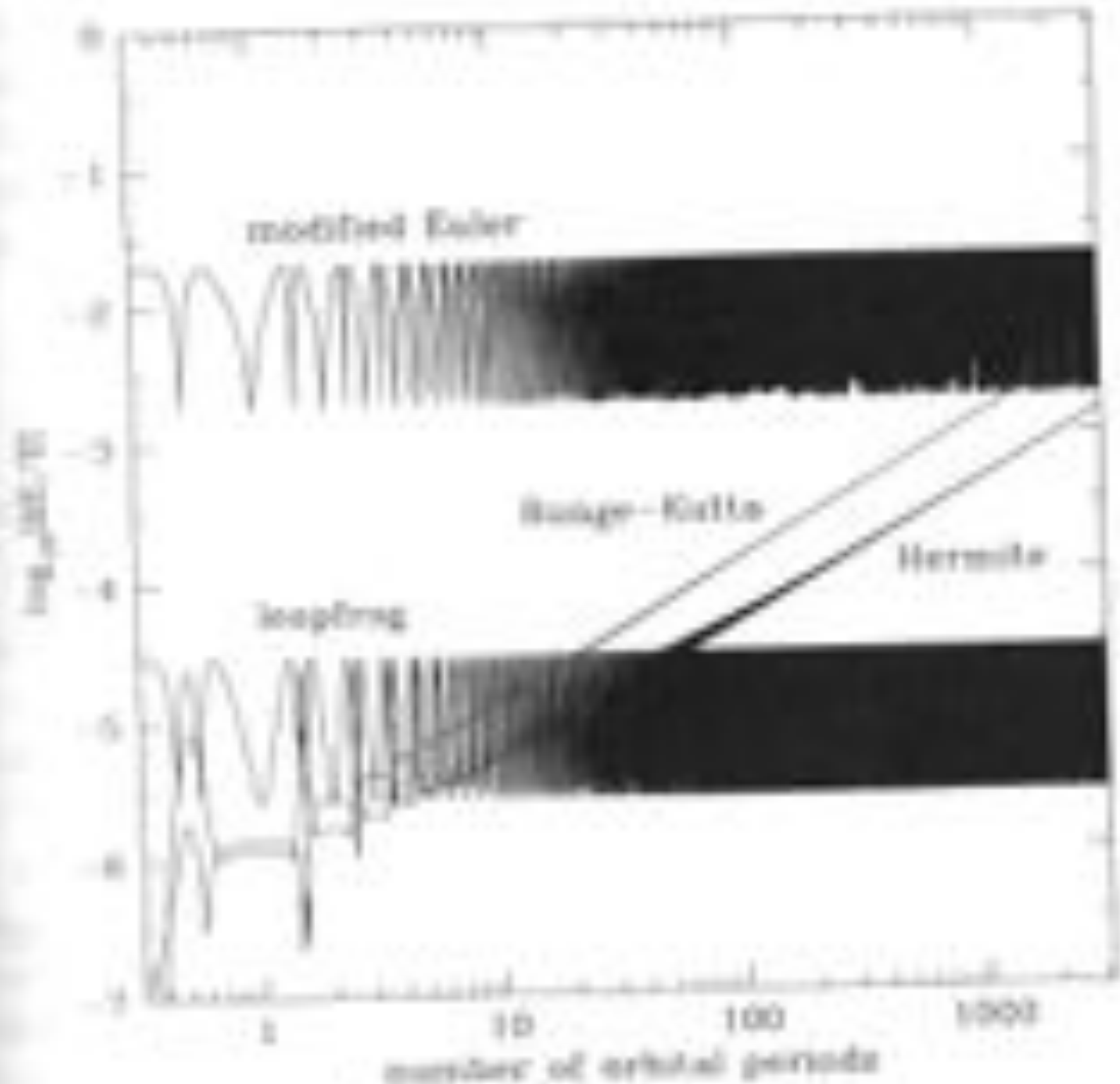

Figure 3.21 Fractional energy error as a function of time for several integrators, following a particle orbiting in the logarithmic potential $\Phi(r) = \ln r$. The orbit is moderately eccentric (apocenter twice as big as pericenter). The timesteps are fixed, and chosen so that there are 200 evaluations of the force or its derivatives per period for all of the integrators. The integrators shown are kick-drift modified Euler (3.163a), leapfrog (3.166a), Runge-Kutta (3.169), and Hermite (3.172a-d). Note that (i) over moderate time intervals, the errors are smallest for the fourth-order integrators (Runge-Kutta and Hermite), intermediate for the second-order integrator (leapfrog), and largest for the first-order integrator (modified Euler); (ii) the energy error of the symplectic integrators does not grow with time.